REPORT DOCUMENTATION PAGE

Form Approved
OMB NO. 0704-0188

Public Reporting burden for this collection of information is estimated to average 1 hour per response, including the time for reviewing instructions, searching existing data sources, gathering and maintaining the data needed, and completing and reviewing the collection of information. Send comment regarding this burden estimates or any other aspect of this collection of information, including suggestions for reducing this burden, to Washington Headquarters Services, Directorate for information Operations and Reports, 1215 Jefferson Davis Highway, Suite 1204, Arlington, VA 22202-4302, and to the Office of Management and Budget, Paperwork Reduction Project (0704-0188,) Washington, DC 20503.

1. AGENCY USE ONLY (Leave Blank)	2. REPORT DATE 05/17/2002	3. REPORT TYPE AND DATES COVERED Final, July 2001 - May, 2002
4. TITLE AND SUBTITLE Experimental Ammonia-Based Power Systems		5. FUNDING NUMBERS DAAD19-01-C-0076
6. AUTHOR(S) Steve Schmit		
7. PERFORMING ORGANIZATION NAME(S) AND ADDRESS(ES) Gradient Technology		8. PERFORMING ORGANIZATION REPORT NUMBER
9. SPONSORING /MONITORING AGENCY NAME(S) AND ADDRESS(ES) U. S. Army Research Office P.O. Box 12211 Research Triangle Park, NC 27709-2211		20030310 038 42692.1 CH-11

11. SUPPLEMENTARY NOTES
The views, opinions and/or findings contained in this report are those of the author(s) and should not be construed as an official Department of the Army position, policy or decision, unless so designated by other documentation.

12 a. DISTRIBUTION /AVAILABILITY STATEMENT Approved for public release; distribution unlimited.	12 b. DISTRIBUTION CODE

13. ABSTRACT (Maximum 200 words)

Gradient Technology has investigated a small-scale experimental ammonia-based power system. The system is composed of two primary components. The first component, a hydrogen-generating catalytic reactor, operates through the autothermal decomposition of ammonia at large space velocities. Since reactor volume is inversely proportional to space velocity, small amounts of catalyst can process large amounts of ammonia. *Gradient Technology* utilizes space velocities in excess of 5×10^5 hr^{-1}. As a result, a catalyst bed volume of 0.2 cm^3 is required to produce 4.0×10^{-2} mole H_2 min^{-1} from 3.8×10^{-2} mole NH_3 min^{-1} and 4.5×10^{-2} mole air min^{-1} in a reactor that weighs 325 grams and has volume of 150 cm^3 (excluding flow controllers and ammonia storage). The second component, a commercial hydrogen/air PEM fuel cell, utilizes the hydrogen generated in the catalytic reactor to generate approximately 30 Watts of electrical power. *Gradient Technology* has also investigated the storage of anhydrous ammonia (130 gram aliquots) for the purpose of addressing the portability and safety of ammonia-based power systems. Lastly, the adsorption of ammonia on zeolite materials and activated carbon has been investigated for the purpose of removing residual ammonia from the reactor effluent stream and adsorbing ammonia from a rupture of an ammonia storage vessel.

14. SUBJECT TERMS autothermal, ammonia, fuel cell			15. NUMBER OF PAGES 80 16. PRICE CODE
17. SECURITY CLASSIFICATION OR REPORT **UNCLASSIFIED**	18. SECURITY CLASSIFICATION ON THIS PAGE **UNCLASSIFIED**	19. SECURITY CLASSIFICATION OF ABSTRACT **UNCLASSIFIED**	20. LIMITATION OF ABSTRACT **UL**

NSN 7540-01-280-5500

Standard Form 298 (Rev.2-89)
Prescribed by ANSI Std. 239-18
298-102

(This page is intentionally left blank.)

MASTER COPY: PLEASE KEEP THIS "MEMORANDUM OF TRANSMITTAL" BLANK FOR REPRODUCTION PURPOSES. WHEN REPORTS ARE GENERATED UNDER THE ARO SPONSORSHIP, FORWARD A COMPLETED COPY OF THIS FORM WITH EACH REPORT SHIPMENT TO THE ARO. THIS WILL ASSURE PROPER IDENTIFICATION. NOT TO BE USED FOR INTERIM PROGRESS REPORTS; SEE PAGE 2 FOR INTERIM PROGRESS REPORT INSTRUCTIONS.

MEMORANDUM OF TRANSMITTAL

U.S. Army Research Office
ATTN: AMSRL-RO-RI (Hall)
P.O. Box 12211
Research Triangle Park, NC 27709-2211

- ☐ Reprint (Orig + 2 copies)
- ☐ Manuscript (1 copy)
- ☐ Technical Report (Orig + 2 copies)
- ☐ Final Progress Report (Orig + 2 copies)
- ☐ Related Materials, Abstracts, Theses (1 copy)

CONTRACT/GRANT NUMBER:

REPORT TITLE:

is forwarded for your information.

SUBMITTED FOR PUBLICATION TO (applicable only if report is manuscript):

Sincerely,

(This page is intentionally left blank.)

Contents

I.	Introduction		1
II.	Technical Background		4
	A.	Commercial Ammonia Manufacturing	4
	B.	Ammonia Decomposition	18
	C.	Ammonia Adsorption	28
	D.	Ammonia Storage	31
	E.	PEM Fuel Cells	31
III.	Experimental		35
	A.	Materials	35
	B.	Equipment and Procedures	38
IV.	Results and Discussion		49
	A.	Reactor Performance	49
	B.	Fuel Cell Testing	56
	C.	Ammonia Adsorption	58
	D.	Ammonia Storage	64
V.	Conclusions		65
VI.	References		66

(This page is intentionally left blank.)

List of Figures

Figure 1. Hydrogen mass fraction and hydrogen density for ammonia and various carbon-based fuels. States of aggregation: ammonia (liquid at 294 K and 889 kPa), ammonia (liquid at 344 K and 3398 kPa), methanol (liquid at 298 K and 101 kPa), methane and ethane (gas at 298 K and 6893 kPa), butane through hexadecane (liquid at 298 K and 101 kPa), and octadecane and eicosane (solid at 298 K and 101 kPa).

Figure 2. Ammonia processing components illustrating the simplicity of the system.

Figure 3. Syngas generation from natural gas and other light hydrocarbons.

Figure 4. Syngas generation from not only light hydrocarbons but also heavier hydrocarbons and coal.

Figure 5. Phase equilibria for syngas generation from hydrocarbons at 360 psig and 1800°F.

Figure 6. Flowsheet of Haber-Bosch-Mittasch synthesis process.[2]

Figure 7. Chemical equilibrium constant for the synthesis of ammonia from a stoichiometric mixture of hydrogen and nitrogen as a function of temperature.

Figure 8. Equilibrium extent of reaction for the synthesis of ammonia from a stoichiometric mixture of hydrogen and nitrogen.

Figure 9. Two possible routes to hydrogen from ammonia.

Figure 10. Chemical equilibrium constant for the decomposition of ammonia from pure ammonia as a function of temperature.

Figure 11. Equilibrium extent of reaction for the decomposition of pure ammonia.

Figure 12. Adiabatic flame temperature and ammonia conversion for ammonia/air mixtures fed at 25°C with complete oxygen consumption.

Figure 13. Chemical equilibrium constant for the decomposition of ammonia and the formation of nitrogen oxides as a function of temperature.

Figure 14. Autothermal ammonia decomposition conducted in an experimental quartz reactor.

List of Figures

Figure 15. Experimental single-pass straight-tube reactor for the autothermal ammonia decomposition.

Figure 16. Experimental two-pass coaxial reactor for the autothermal ammonia decomposition.

Figure 17. Adsorption isotherm for ammonia on activated carbon at 25°C.

Figure 18. Ammonia vapor pressure curve.[1]

Figure 19. Nickel nitrate solution with foam monoliths.

Figure 20. Reactor base back view.

Figure 21. Reactor base side view (center slice).

Figure 22. Reactor base front view.

Figure 23. Hydrogen-generating catalytic reactor.

Figure 24. Micro air pump used to deliver air to the hydrogen-generating catalytic reactor.

Figure 25. Single cell PEM fuel cell coupled to the hydrogen-generating catalytic reactor.

Figure 26. Experimental 50 Watt PEM fuel cell.

Figure 27. Quantachrome Autosorb 1-C Chemisorption-Physisorption Analyzer used to collect ammonia adsorption isotherms.

Figure 28. Ammonia storage canister.

Figure 29. Ruthenium foam monolith catalyst performance in the two-pass coaxial quartz reactor.

Figure 30. Ruthenium sphere bed catalyst performance in the two-pass coaxial quartz reactor.

Figure 31. Nickel foam monolith catalyst performance in the two-pass coaxial quartz reactor.

Figure 32. Nickel sphere bed catalyst performance in the two-pass coaxial quartz reactor.

List of Figures

Figure 33. Nickel woven gauze catalyst performance in the two-pass coaxial quartz reactor.

Figure 34. Nickel sphere bed catalyst performance in the alumina tube reactor.

Figure 35. AA Micro air pump performance data.

Figure 36. AAA Micro air pump performance data.

Figure 37. Power output of the PEM fuel cell stack.

Figure 38. Ammonia adsorption isotherm at 25°C on type 3A zeolite.

Figure 39. Ammonia adsorption isotherm at 100°C on type 3A zeolite.

Figure 40. Ammonia adsorption isotherm at 25°C on type 13X zeolite.

Figure 41. Ammonia adsorption isotherm at 100°C on type 13X zeolite.

Figure 42. Ammonia adsorption isotherm at 25°C on activated carbon.

Figure 43. Ammonia adsorption isotherm at 100°C on activated carbon.

List of Tables

Table 1. Main Thermodynamic Properties of H_2, N_2, and O_2

Table 2. Main Thermodynamic Properties of NH_3 and H_2O

Table 3. Feed Gas Equations

Table 4. Reactor Performance Equations

Table 5. Thermodynamic Analysis of H_2/O_2 Electrochemical Cell

Table 6. Metal Salt Solutions Used for Supported Catalyst Preparation

Table 7. Candidate Materials for Ammonia Adsorption

Table 8. Material Properties for Cast and Extruded Alumina Tubes

Table 9. Micro Air Pump Specifications

Table 10. Reactor Performance for Fuel Cell Test

Table 11. Reactor Performance Equations

I. INTRODUCTION

In the project entitled "Experimental Ammonia-Based Power Systems" *Gradient Technology* investigated a system composed of a hydrogen-generating catalytic reactor and a hydrogen/air proton-exchange membrane (PEM) fuel cell. The hydrogen-generating catalytic reactor utilizes a heterogeneous catalyst to convert an ammonia/air gas stream to a hydrogen-rich gas stream with minimal energy input. After the hydrogen-rich gas stream is polished to remove residual ammonia, it is sent to a PEM fuel cell for electrical power generation. This project focused on assessing the performance of the catalytic reactor and its utility in providing the necessary hydrogen to drive a 30 Watt PEM fuel cell. In addition, *Gradient Technology* assessed the storage of anhydrous ammonia from the standpoint of portability and safety, and gathered data on the adsorption of ammonia on various zeolites and activated carbon. Adsorption data is useful for two primary reasons. First, the catalytic reactor effluent must contain very little residual ammonia (less than 10 ppm) so that efficient adsorption of ammonia on a substrate reduces the mass of adsorbent required to polish the effluent stream for a given period of time. Second, adsorbents can be useful in preventing the release of anhydrous ammonia from storage containers should there be a failure of the container.

At the heart of the experimental ammonia-based power system is the hydrogen-generating catalytic reactor. This reactor utilizes autothermal ammonia reforming chemistry that *Gradient Technology* has studied over the past few years. The term "autothermal" arises when a chemically reactive flow system can sustain reactions without the continuous addition of energy. An advantage of autothermal chemically reactive flow systems is that endothermic chemistry can be driven by exothermic chemistry in the same reaction zone. In autothermal ammonia decomposition the exothermic nature of the combustion of ammonia with air-derived oxygen is used to drive the endothermic cracking of ammonia to produce hydrogen. Thus, ammonia serves as both the supply of heat and hydrogen. Since it is desired to use the hydrogen to generate an electromotive force with a PEM fuel cell, the ammonia can be thought of as a storage mechanism for energy in the form of heat and electricity.

The motivation for conducting the research documented in this report arises from the need for high energy-density sources of power. PEM fuel cell research and development has made significant strides in increasing the energy density of current PEM fuel cells. However, these fuel cells need a hydrogen supply that is free of impurities; impurities can poison PEM fuel cell catalysts used in membrane electrode assemblies (MEAs). Thus, a high energy-density hydrogen source that is free of impurities is required to uphold the high energy-density nature of the PEM fuel cell and to yield a power system with the same attribute.

Traditionally, carbon-based fuels such as methane, gasoline, and diesel fuel are reformed (or partially oxidized) to generate synthesis gas which is subsequently water-gas shifted to drop carbon monoxide concentrations to less than 1 mol %. Lastly, selective oxidation is performed to reduce the carbon monoxide levels to less than 100 ppm. Thus, at least three reaction steps are required to generate a hydrogen stream that still has amounts of carbon monoxide that are detrimental to PEM fuel cell performance. Aside from carbon monoxide, sulfur is another detrimental impurity to the performance of the reformer. As a result, an additional unit operation is required to handle the sulfur. Recent advances in synfuel technology has led to hydrocarbon fuels with extremely low levels of sulfur. Regardless, sulfur-free fuels must be reformed and the carbon monoxide issue still exists.

An inorganic source of hydrogen that eliminates the issues if carbon monoxide and sulfur poisoning is ammonia. Of course, the issue of ammonia poisoning the MEA catalyst now exists,

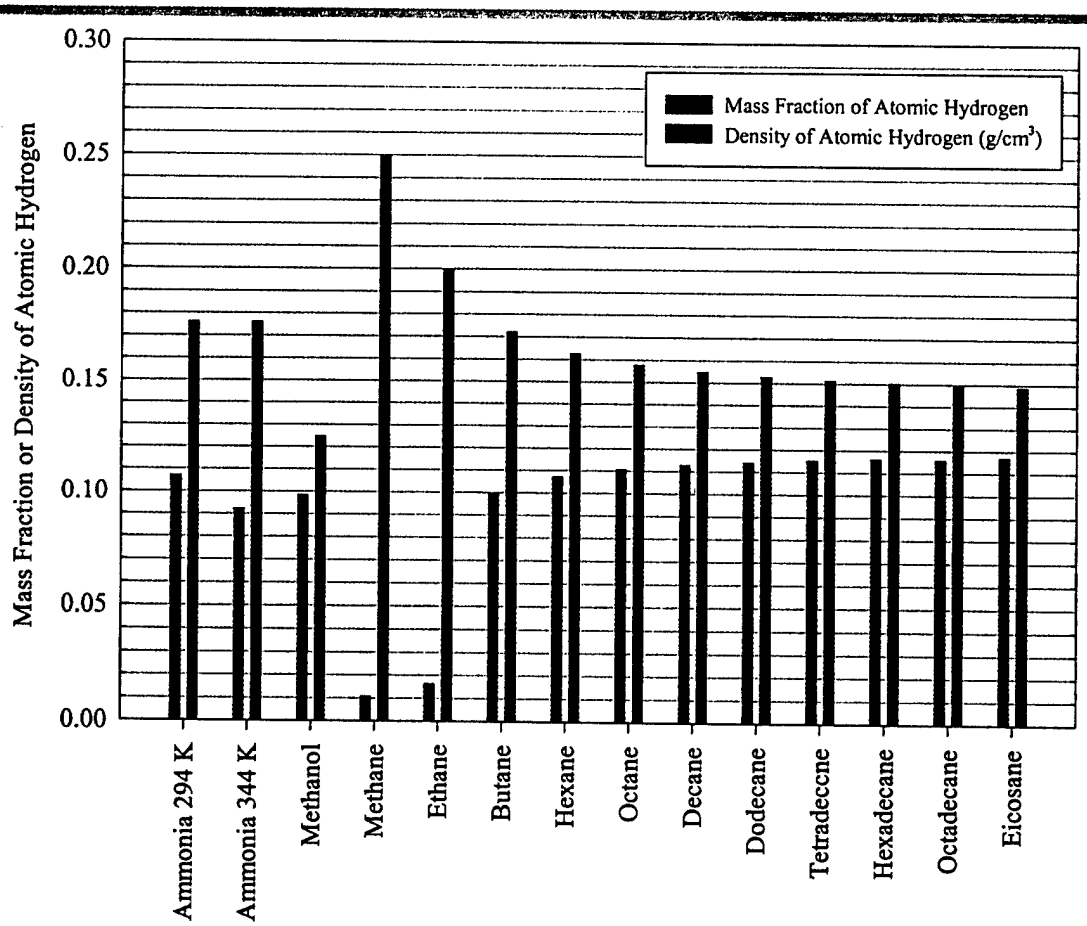

Figure 1. Hydrogen mass fraction and hydrogen density for ammonia and various carbon-based fuels. States of aggregation: ammonia (liquid at 294 K and 889 kPa), ammonia (liquid at 344 K and 3398 kPa), methanol (liquid at 298 K and 101 kPa), methane and ethane (gas at 298 K and 6893 kPa), butane through hexadecane (liquid at 298 K and 101 kPa), and octadecane and eicosane (solid at 298 K and 101 kPa).

however, *Gradient Technology* has shown that removal of ppm levels of ammonia from the effluent of its autothermal ammonia decomposition reactors can be attained with an adsorption bed of zeolite or activated carbon. In addition, an ammonia-based hydrogen source looks attractive when compared to carbon-based hydrogen sources on the basis of hydrogen mass fraction and hydrogen density. Figure 1 compares ammonia to various carbon-based fuels in terms of these two metrics. In terms of mass fraction ammonia contains more hydrogen (17.6% at 294 K [70°F] and 889 kPa [129 psia]) than methanol (12.5%) and alkanes containing four or more carbons (~15%) but less than lighter alkanes (20% - 25%). In terms of density ammonia contains significantly more hydrogen (0.11 g/cm3 at 294 K [70°F] and 889 kPa [129 psia]) than the lighter alkanes (0.02 g/cm^3 at 294 K [70°F] and 6893 kPa [1000 psia]) and is comparable to heavier alkanes (0.12 g/cm^3) and methanol (0.10 g/cm^3). Also note that ammonia exists in the liquid state of aggregation at 129 psia at 70°F whereas methane at 1000 psia still exists as a gas.

Ammonia thus appears to be a very attractive hydrogen source since its hydrogen content (being directly proportional to energy density) is much larger than gaseous hydrocarbons and methanol and slightly larger than the heavier hydrocarbons. Aside from these two metrics one must consider the

processes involved in converting the fuel into hydrogen. The generation of hydrogen from carbon-based fuels has already been briefly discussed. The point of the discussion was to indicate that a number of chemical reactors and unit operations are required. Fortunately, the autothermal ammonia decomposition process greatly simplifies the overall hydrogen-generating process. This is one of the reasons *Gradient Technology* proposed the use of ammonia for small-scale use. In its simplest form, an autothermal ammonia decomposition system requires *two processes*. The first process is *chemical reaction* where the autothermal ammonia decomposition takes place and the second process is *reactor effluent polishing* where residual ammonia is removed via chemisorption. Figure 2 illustrates this simple ammonia processing system and displays the air intake system for introducing air into the reactor and the ignition system for starting the reactor.

Gradient Technology's work on this project focused on utilizing the chemical reactor used to carry out the autothermal ammonia decomposition to feed a PEM fuel cell. In order to successfully analyze and design a chemical reactor, an understanding of the chemistry, kinetics, thermodynamics, and transport involved with the reactor is a prerequisite. In this report, *Gradient Technology* explores an autothermal ammonia decomposition reactor coupled to a PEM fuel cell.

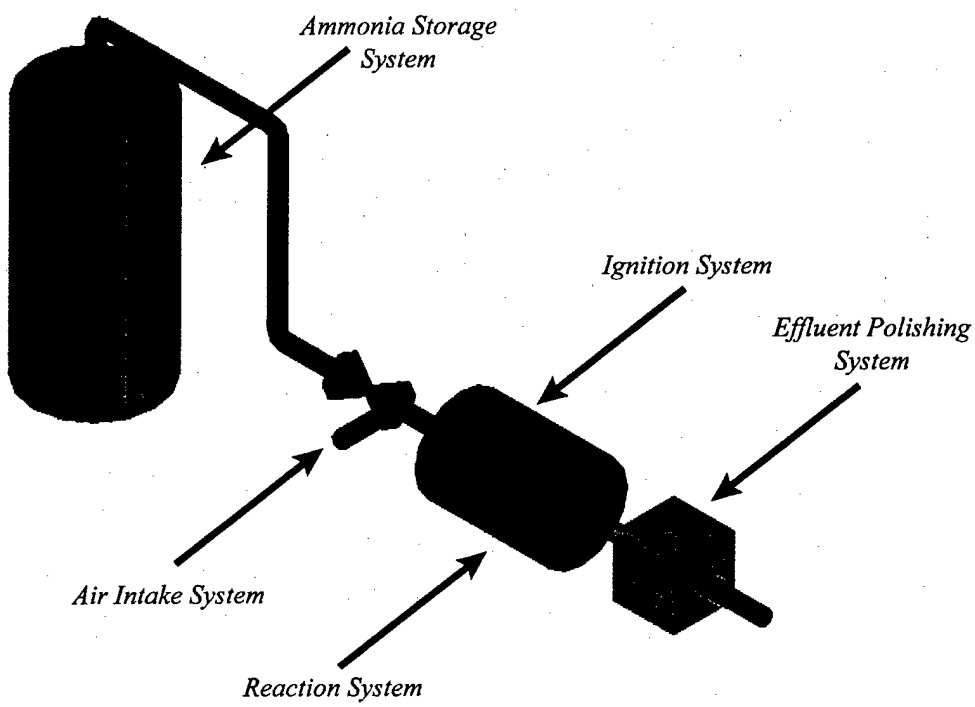

Figure 2. Ammonia processing components illustrating the simplicity of the system.

II. TECHNICAL BACKGROUND

A. Commercial Ammonia Manufacturing

In this report research pertaining to the use of autothermal ammonia decomposition for providing hydrogen to a PEM fuel cell is discussed. Despite the fact that *Gradient Technology* is interested in decomposing ammonia and utilizing the hydrogen to feed a PEM fuel cell, an understanding of the synthesis of ammonia is extremely useful.

1. Syngas Production

The ultimate raw materials for the commercial synthesis of ammonia is a hydrocarbon and air. Typically steam reforming or catalytic partial oxidation is used to generate syngas from natural gas or other light hydrocarbons (natural gas liquids, liquified petroleum gas, naphtha, *etc.*). If heavy fuel oil or vacuum residue is the desired feedstock then non-catalytic partial oxidation techniques are used to generate the ammonia synthesis gas. Figure 3 illustrates the possible steps for generating ammonia synthesis gas from natural gas or other light hydrocarbons. Figure 4 illustrates the possible steps for generating the syngas from not only light hydrocarbons but also heavier hydrocarbons and coal.

The first important step in syngas production is the removal of sulfur from the hydrocarbon feedstock. Desulfurization takes place through the adsorption of sulfur-containing compounds on activated carbon or molecular sieves or by the catalytic hydrogenation of organic sulfur compounds (benzothiophene and dibenzothiophene for example) and subsequent adsorption of hydrogen sulfide on zinc oxide.

Following desulfurization the primary reformer converts the hydrocarbon feed along with steam to syngas via the following set of reactions that occur over a nickel-based catalyst in a tubular reactor operated at 750 - 820°C and 25 - 35 bar:

$$C_nH_m + nH_2O \rightarrow nCO + (m/2 + n)H_2 \qquad (\Delta H^0_{rxn} > 0) \qquad (1)$$

$$CH_4 + H_2O \rightleftarrows CO + 3H_2 \qquad (\Delta H^0_{rxn} = 206\ kJ/mol) \qquad (2)$$

$$CO + H_2O \rightleftarrows CO_2 + H_2 \qquad (\Delta H^0_{rxn} = -41\ kJ/mol) \qquad (3)$$

In this set of reactions higher hydrocarbons react irreversibly and completely with steam (equation 1), however, the final gas composition is governed by the reversible methanation reaction (equation 2) and the reversible water-gas shift reaction (equation 3). Methane conversion is favored by high temperature, low pressure, and high steam content. Since the overall process described above is endothermic, heat is added to the process; the reactor thus consists of tubes heated externally through fuel combustion.

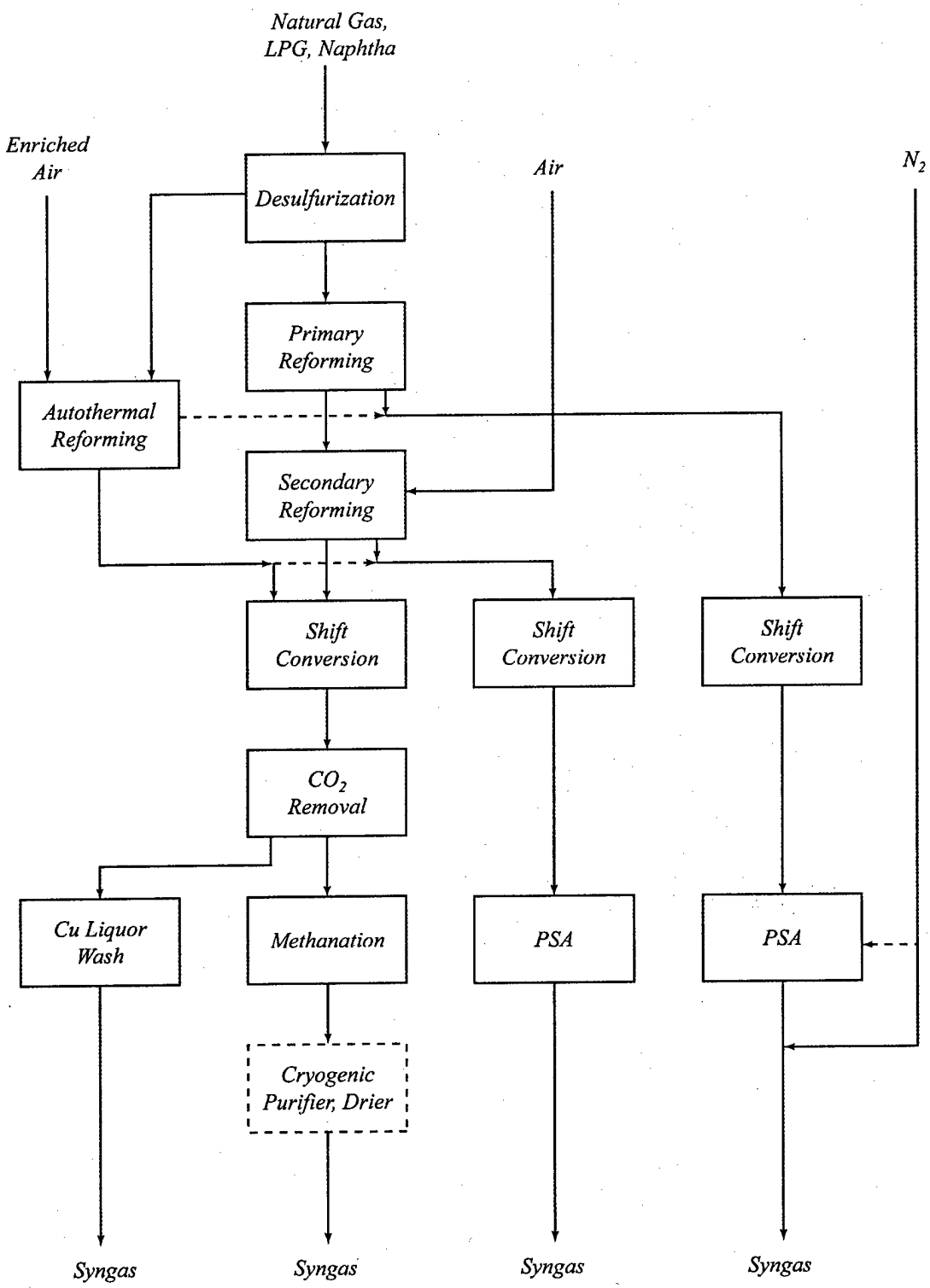

Figure 3. Syngas generation from natural gas and other light hydrocarbons.

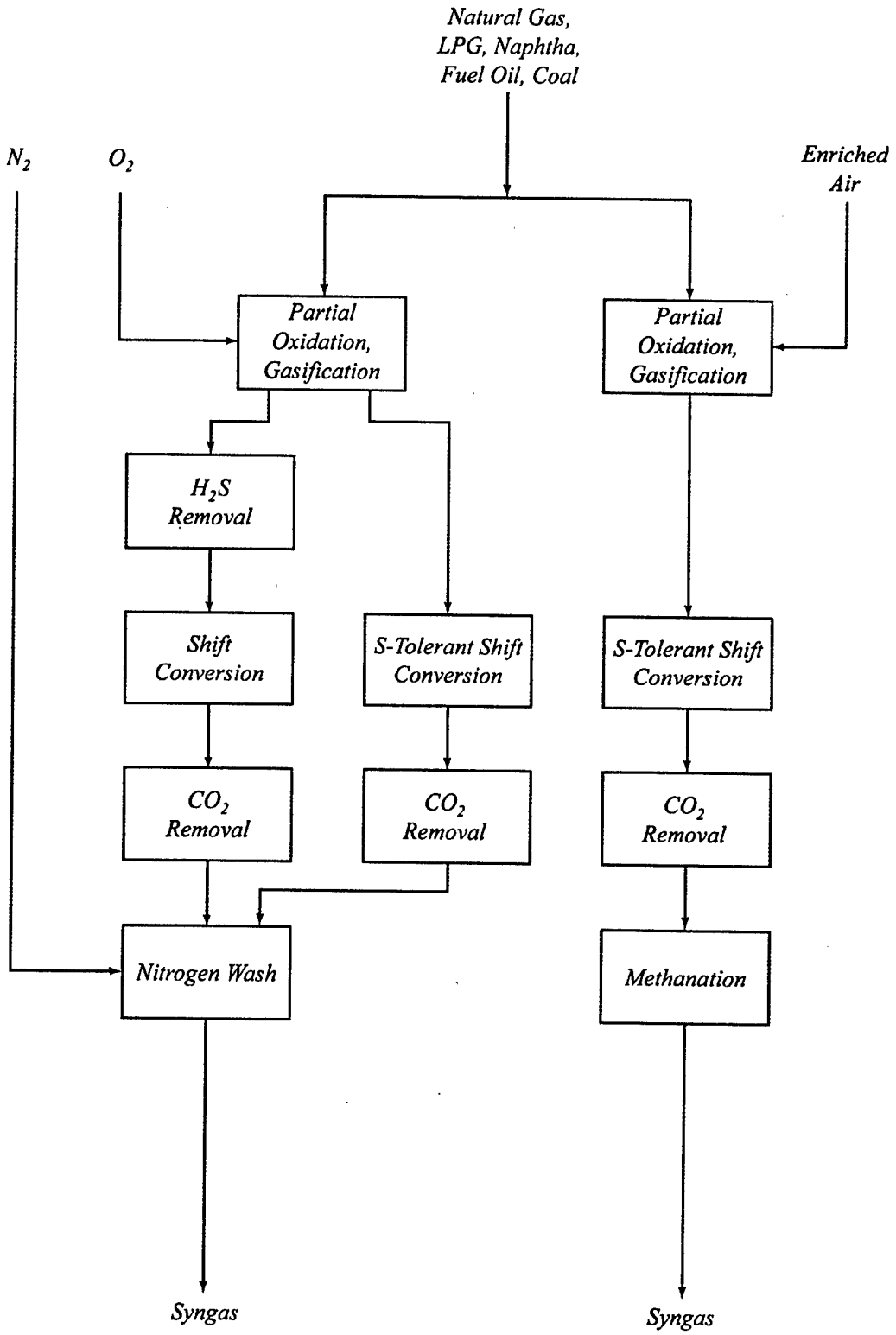

Figure 4. Syngas generation from not only light hydrocarbons but also heavier hydrocarbons and coal.

In primary reforming operations there is always the risk of carbon formation via the following reactions:

$$C_nH_m \rightleftarrows nC + m/2\,H_2 \qquad (\Delta H^0_{rxn} > 0) \qquad (4)$$

$$2CO \rightleftarrows C + CO_2 \qquad (\Delta H^0_{rxn} = -172) \qquad (5)$$

$$CO + H_2 \rightleftarrows C + H_2O \qquad (\Delta H^0_{rxn} = -131) \qquad (6)$$

Note that when $n = 1$ and $m = 4$ (methane) equation 2 (methane-steam reforming) becomes a linear combination of equation 4 and equation 6. Also, equation 3 (water-gas shift) is a linear combination of equation 5 and equation 6.

It is important to understand phase equilibria for carbon, hydrogen, and oxygen when defining the startup, operational, and shutdown conditions for a reforming (or partial oxidation) reactor. Figure 5 depicts the phase equilibria for syngas generation from hydrocarbons at 360 psig and 1800°F. In this figure the line connecting point 1 and point 2 is the phase equilibrium line in which the two-phase solid-gas region lies to the left of the phase equilibrium line and the single-phase gas region lies to the right. Point 3 in figure 5 represents pure methane and point 4 represents atomic oxygen. The line connecting these two points (the composition line) represents various methane:oxygen ratios and through the use of the lever rule indicates that methane:oxygen ratios less than 5 are required to remain in the single-phase gas region. Thus, as an example, any operation that places the reactor composition (at 360 psig and 1800°F) to the left of the phase equilibrium line will favor the deposition of carbon.

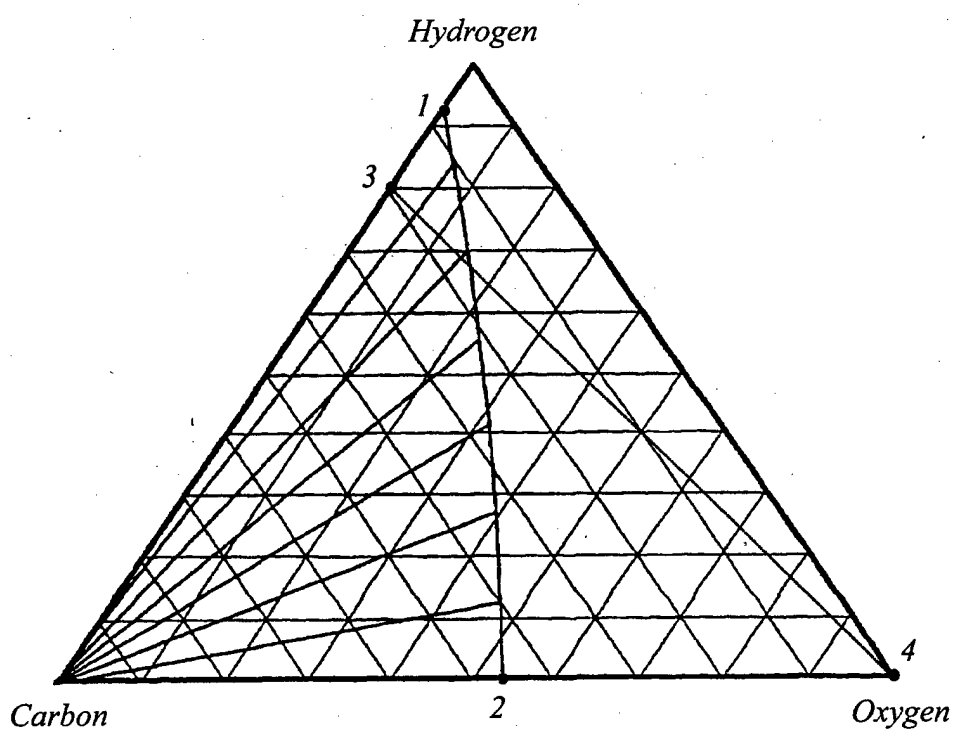

Figure 5. Phase equilibria for syngas generation from hydrocarbons at 360 psig and 1800°F.

Unlike the overall endothermicity of the reaction system in the primary reformer, the secondary reformer is operated adiabatically in which the effluent from the primary reformer is mixed with air and reacted over another nickel-based catalyst. It is the intent of the secondary reformer to not only reduce the methane content to a low level, but also introduce the necessary nitrogen for the ammonia synthesis step. Typically air is introduced at a rate such that the nitrogen:hydrogen ratio in the ammonia synthesis gas is 3. The secondary reformer generally operates at 950 - 1025°C and 25 - 35 bar.

An alternative to the primary and secondary reforming processes is the autothermal reforming process (or catalytic partial oxidation process) in which the reaction is carried out in a reactor similar to the secondary reformer but contains various reaction zones and utilizes air, oxygen-enriched air, or oxygen as the oxidizing agent.

Two other techniques have also been used to generate ammonia synthesis gas. These techniques, non-catalytic partial oxidation and gasification, can utilize light hydrocarbon feedstocks, however, they are especially suited for heavier hydrocarbon feedstocks including naphtha, heavy oil, coal, and lignite.

Non-catalytic partial oxidation processes react a hydrocarbon feedstock with oxygen or oxygen-enriched air at high temperatures and pressures (usually in excess of 1300°C and 60 bar) to yield a gas composed of hydrogen, carbon oxides, some steam, and traces of methane and hydrogen sulfide. Since the process is relatively insensitive to sulfur, the desulfurization step is usually bypassed.

The non-catalytic partial oxidation process is chemically complex but can be represented in a simplified form as follows:

$$C_nH_m + nH_2O \rightarrow nCO + (m/2 + n)H_2 \qquad (\Delta H^0_{rxn} > 0) \qquad (7)$$

$$C_nH_m + n/2\,O_2 \rightarrow nCO + m/2\,H_2 \qquad (\Delta H^0_{rxn} < 0) \qquad (8)$$

$$CH_4 + H_2O \rightleftarrows CO + 3H_2 \qquad (\Delta H^0_{rxn} = 206\ kJ/mol) \qquad (9)$$

$$CO + H_2O \rightleftarrows CO_2 + H_2 \qquad (\Delta H^0_{rxn} = -41\ kJ/mol) \qquad (10)$$

$$C_nH_m \rightleftarrows nC + m/2\,H_2 \qquad (\Delta H^0_{rxn} > 0) \qquad (11)$$

Equation 7 and equation 8 irreversibly react the hydrocarbon with oxygen and steam whereas equation 9 (methanation) and equation 10 (water-gas shift) approach equilibrium. As in steam reforming and catalytic partial oxidation, carbon formation can be a problem and must also be examined carefully.

Gasification techniques used to generate syngas from solid feedstocks such as coal and lignite are attractive in some parts of the world where these materials are abundant. In general, gasification processes react coal or lignite with oxygen and steam in a fluidized bed. Numerous variations of these processes exist including the Koppers-Totzek and Winkler processes (low pressure) and the Lurgi and Texaco processes (high pressure).

Regardless of the process used to generate syngas (steam reforming, catalytic partial oxidation, non-catalytic partial oxidation, or gasification) the effluent from these reactors contains significant amounts of carbon monoxide and carbon dioxide. The ammonia synthesis process requires the removal of these two compounds. Carbon monoxide is removed via the water-gas shift reaction and selective oxidation. Carbon dioxide, on the other hand, is removed via an acid gas removal process.

2. Shift Conversion

The water-gas shift process occurs through the following reaction:

$$CO + H_2O \rightleftarrows CO_2 + H_2 \qquad (\Delta H^0_{rxn} = -41\ kJ/mol) \qquad (12)$$

Several catalysts and processes exist for water-gas shift. The classical process uses a magnetite catalyst promoted with chromia. Reactor temperatures are in excess of 350°C and reduce carbon monoxide concentrations to approximately 3 vol % on a dry basis. This step is usually referred to as high temperature shift conversion. A second shift conversion step is then performed with a copper-based catalyst at temperatures around 200°C. This second shift conversion step reduces carbon monoxide to levels around 0.1 - 0.3 vol % on a dry basis and is referred to as low temperature shift conversion. Low temperature shift catalysts are, however, extremely sensitive to poisoning by chlorine and sulfur.

3. Selective Oxidation

The next attempt to further reduce carbon monoxide levels in ammonia synthesis gas is conducted in a selective oxidation reactor. In the selective oxidation process, effluent from the low temperature shift reactor is cooled and condensate is removed. Next, a small amount of air is mixed with the cool stream and is passed into the selective oxidation reactor that contains a precious metal catalyst. Upon contact with the catalyst, the carbon monoxide reacts with the oxygen and the excess oxygen reacts with hydrogen. Carbon monoxide levels can be reduced to approximatley 100 vol ppm with the selective oxidation step.

4. Acid Gas Removal

Before ammonia synthesis gas can be fed to the synthesis reactor, oxygen-containing compounds must be reduced to low ppm levels since these compounds are poisons to ammonia synthesis catalysts. As a result, carbon monoxide, carbon dioxide, and water must be removed from the ammonia synthesis gas.

The steam reforming of light hydrocarbons followed by shift conversion yields a gas stream that contains about 18 vol % carbon dioxide on a dry basis. Even larger carbon dioxide concentrations are present in the ammonia synthesis gas if heavy hydrocarbons or solid feedstocks are processed via non-catalytic partial oxidation or gasification processes. The carbon dioixde as well as any remaining sulfur compounds are removed with acid gas removal units in which acid gases are absorbed (physically or chemically) in a solvent.

The acid gas removal units are essentially absorption vessels with trays or packing that hold the absorbent solution; these vessels operate at synthesis gas pressure. The rich solution is regenerated in a separate vessel at reduced pressure through a stripping and/or a reboiling process. The acid gas removal units can drop the carbon dioxide level in the ammonia synthesis gas to less than 1000 vol ppm.

In acid gas removal units based upon chemical absorption, the most common solvents used are monoethanolamine or hot solutions of potassium carbonate. In units based upon physical absorption various solvents including water, methanol, and propylene carbonate have been used.

5. Copper Liquor Wash

The copper liquor wash is the oldest process used in the final purification of ammonia synthesis gas. This process removes carbon monoxide and carbon dioxide to the required low levels through absorption in a solution comprised of cuprammonium salts of acetic, formic, or carbonic acid. The advantage of this process is that carbon oxides are removed by absorption rather than by a hydrogen-consuming reaction such as methanation. The main disadvantages of this process are that it is rather difficult to operate, consumes large amount of energy, and can pollute the environment.

6. Cryogenic Purification

In ammonia plants based on the partial oxidation of heavy oil or gasification of coal, cryogenic purification is used as the final synthesis gas purifier. In a cryogenic purification unit the synthesis gas is partially condensed to remove the excess nitrogen introduced into the secondary reformer. In addition some of the inerts (methane, argon, *etc.*) are also removed. The resulting synthesis gas is completely dry and has a low inerts content.

7. Pressure Swing Absorption

Pressure swing absorption technology is commmonly used in plants based on steam reforming for hydrogen purification. This technology has the advantage that it can replace both the acid gas removal process and the cryogenic purification process. In pressure swing adsorption, hydrogen can be adsorbed onto carbon or a zeolite at high pressure and subsequently desorbed at low pressure.

8. Methanation

Methanation is the most important process for the removal of the last traces of carbon monoxide and carbon dioxide from ammonia synthesis gas. Methanation reacts carbon oxides to extinction (less than 10 vol ppm) at 250 - 350°C over a nickel catalyst via the following reactions:

$$CO + 3H_2 \rightarrow CH_4 + H_2O \qquad (\Delta H^0_{rxn} = -206\ kJ/mol) \qquad (13)$$

$$CO_2 + 4H_2 \rightarrow CH_4 + H_2O \qquad (\Delta H^0_{rxn} = 76.8\ kJ/mol) \qquad (14)$$

Methanation is a simple, reliable, and inexpensive process, however, it consumes a certain amount of hydrogen.

9. Ammonia Synthesis Loop

Ammonia is commercially synthesized by contacting hydrogen and nitrogen with a supported metal catalyst contained in a reactor train operated at temperatures in excess of 500°C. The reaction stoichiometry is as follows:

$$N_2 + 3H_2 \rightleftarrows 2NH_3 \qquad (\Delta H^0_{rxn} = -92.38\ kJ/mol) \qquad (15)$$

The aforementioned eight processing steps yield ammonia synthesis gas at a composition of three moles of hydrogen for each mole of nitrogen. Before the ammonia synthesis gas is fed to the synthesis loop, the synthesis gas must be compressed, however, to pressures in excess of 100 bar. Since the conversion of synthesis gas to ammonia is equilibrium limited, interstage separation and heat exchange along with recycle is required.

There are a number of ammonia synthesis loop designs that have been used commercially. The more common ones include the Fauser synthesis process, Haber-Bosch-Mittasch process, N.E.C. process, Uhde process, Casale process, and the Claude process. The Haber-Bosch-Mittasch process is shown in figure 6.

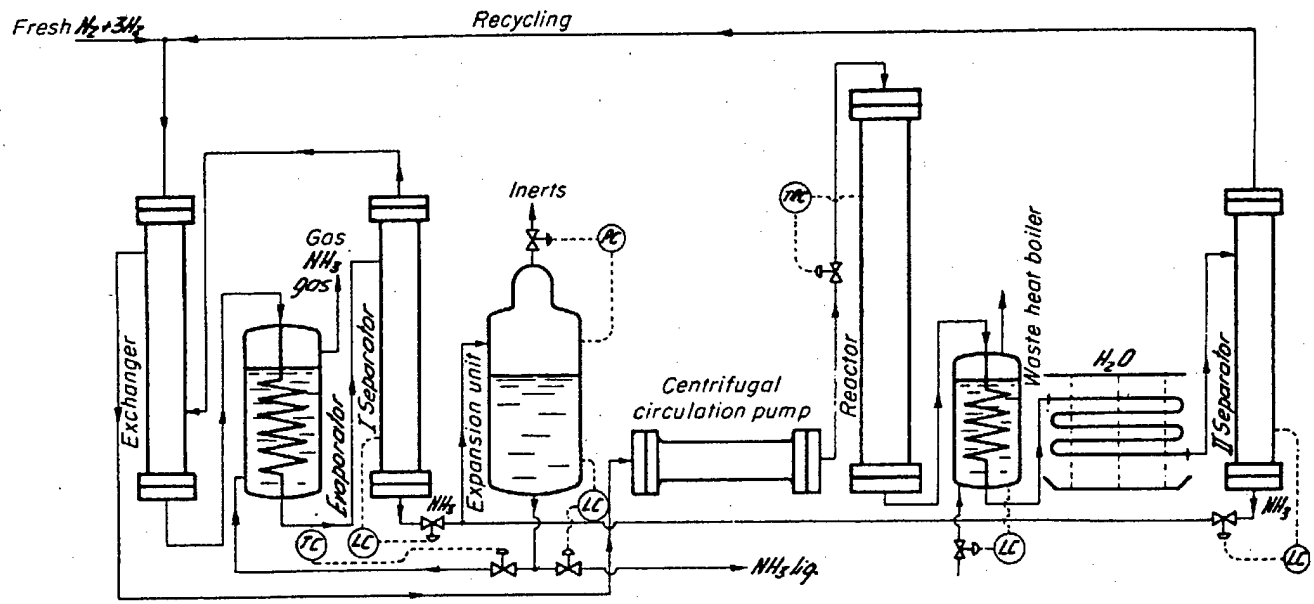

Figure 6. Flowsheet of Haber-Bosch-Mittasch synthesis process.[1]

In the Haber-Bosch-Mittasch process the working pressure varies from approximately 215 bar in older plants to 320 bar in more modern plants. In this process fresh synthesis gas first passes through a precatalysis system and is subsequently distributed to the production units. The precatalysis unit, which uses the same catalyst as the other units, simplifies the preceeding copper liquor wash. Separation of the ammonia is through cooling to $-20°C$. The catalyst used in this process is typically $Fe\text{-}Al_2O_3\text{-}K_2O$ and is generally obtained from natural magnetite with a low SiO_2 content. Space velocities in the ammonia synthesis reactors range from 8000 to 10000 Nm^3/hm^3. The ammonia content of the reactor effluent ranges from 13 vol % to 15 vol % whereas the ammonia content after separation is around 1.5 vol %. The average reactor temperature ranges from 530 - 560°C.

10. Thermodynamics of the Ammonia Synthesis

The chemical equilibrium constant for the ammonia synthesis reaction was first determined at atmospheric pressure by Haber,[2] at medium pressure by Nernst,[3] and at high pressure by Haber.[2] Table 1 and table 2 give the main thermodynamic characteristics of hydrogen, nitrogen, and ammonia as well as oxygen and water. From this information it can be seen that the standard Gibbs free energy of formation of ammonia is negative indicating that ammonia tends to be formed at 298K and 1 bar. The expression for evaluating the equilibrium extent of reaction takes the following form:

$$K_a = \xi(2-\xi)\left[1/2(1-\xi)\right]^{-1/2}\left[3/2(1-\xi)\right]^{-3/2}\left[P_{rxn}/1\text{ bar}\right]^{-1}K_v \qquad (16)$$

The chemical equilibrium constant, K_a, can be evaluated from thermodynamic information and the following definition:

$$K_a(T) = \exp\left(-\Delta G^0/RT\right) \qquad (17)$$

Figure 7 plots the chemical equilibrium constant as a function temperature for the ammonia synthesis reaction as calculated with equation 17 and figure 8 plots the equilibrium extent of reaction as a function of pressure and temperatrute as calculated with equation 16. For the calculations used to generate figure 8, the fugacity coefficient equilibrium ratio, K_v, in equation 16 is set to unity (ideal gas assumption). This assumption simplifies the calculation procedure and yields results that illustrate qualitatively the effects of pressure and temperature. However, at typical ammonia synthesis pressures and temperatures, gas phase nonidealities exist and more rigorous calculations are necessary. Nonetheless, figure 8 reveals that the ammonia synthesis should be carried out at as low a temperature and as high a pressure as possible. Economic factors, however, limit the convenience of operating at a very high pressure. Also, operating at too low a temperature has the disadvantage of reducing the reaction rate. One can immediately realize there is an optimum set of operational conditions for a commercial ammonia synthesis plant that yields the most attractive economic opportunities.

Table 1. Main Thermodynamic Properties of H_2, N_2, and O_2

Hydrogen

Critical temperature:	33.3 K
Critical pressure:	12.8 atm

Note that at a critical temperature of 41 K and a critical pressure of 21 atm hydrogen characterisitics become more similar to those of a van der Waals gas. These values should be adopted in the calculation of reduced pressures and temperatures.

Heat capacity at 1 atm in J/mol K from 0°C to 1500°C. Temperature units are in Celsius.

$$C_p = 28.84 + 0.00765\times10^{-2}\,T + 0.3288\times10^{-5}\,T^2 - 0.8698\times10^{-9}\,T^3$$

$\Delta H_f^0 = 0$
$\Delta S_f^0 = 0$
$\Delta G_f^0 = 0$

Nitrogen

Critical temperature:	126.2 K
Critical pressure:	33.5 atm

Heat capacity at 1 atm in J/mol K from 0°C to 1500°C. Temperature units are in Celsius.

$$C_p = 29.00 + 0.2199\times10^{-2}\,T + 0.5723\times10^{-5}\,T^2 - 2.871\times10^{-9}\,T^3$$

$\Delta H_f^0 = 0$
$\Delta S_f^0 = 0$
$\Delta G_f^0 = 0$

Oxygen

Critical temperature:	154.4 K
Critical pressure:	49.7 atm

Heat capacity at 1 atm in J/mol K from 0°C to 1500°C. Temperature units are in Celsius.

$$C_p = 29.10 + 1.158\times10^{-2}\,T - 0.6076\times10^{-5}\,T^2 + 1.311\times10^{-9}\,T^3$$

$\Delta H_f^0 = 0$
$\Delta S_f^0 = 0$
$\Delta G_f^0 = 0$

Table 2. Main Thermodynamic Properties of NH_3 and H_2O

Ammonia (g)

Critical temperature:	405.6 K
Critical pressure:	111.5 atm

Heat capacity at 1 atm in J/mol K from 0°C to 1200°C. Temperature units are in Celsius.

$$C_p = 35.15 + 2.954\times10^{-2}\,T + 0.4421\times10^{-5}\,T^2 - 6.686\times10^{-9}\,T^3$$

$\Delta H_f^0 = -46.19$ kJ/mol
$\Delta S_f^0 = -99.8$ J/mol
$\Delta G_f^0 = -16.45$ kJ/mol

Water (g)

Critical temperature:	126.2 K
Critical pressure:	33.5 atm

Heat capacity at 1 atm in J/mol K from 0°C to 1500°C. Temperature units are in Celsius.

$$C_p = 33.46 + 0.6880\times10^{-2}\,T + 0.7604\times10^{-5}\,T^2 - 3.593\times10^{-9}\,T^3$$

$\Delta H_f^0 = -241.83$ kJ/mol
$\Delta S_f^0 = -44.5$ J/mol
$\Delta G_f^0 = -228.6$ kJ/mol

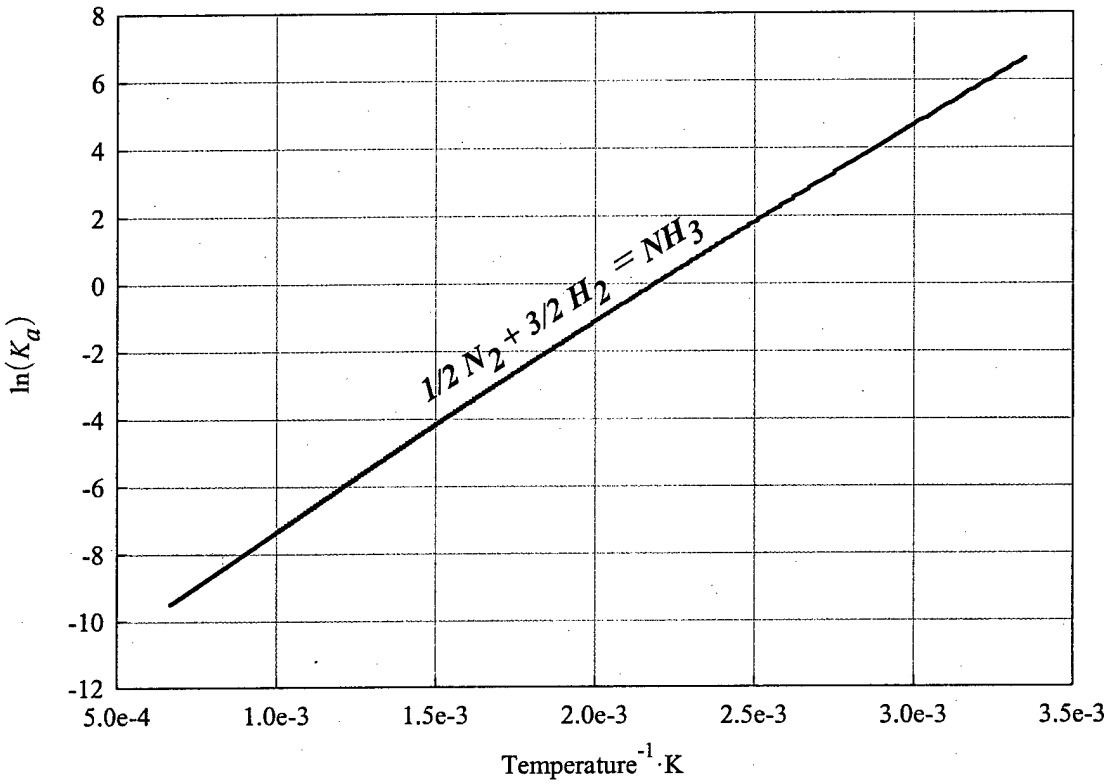

Figure 7. Chemical equilibrium constant for the synthesis of ammonia from a stoichiometric mixture of hydrogen and nitrogen as a function of temperature.

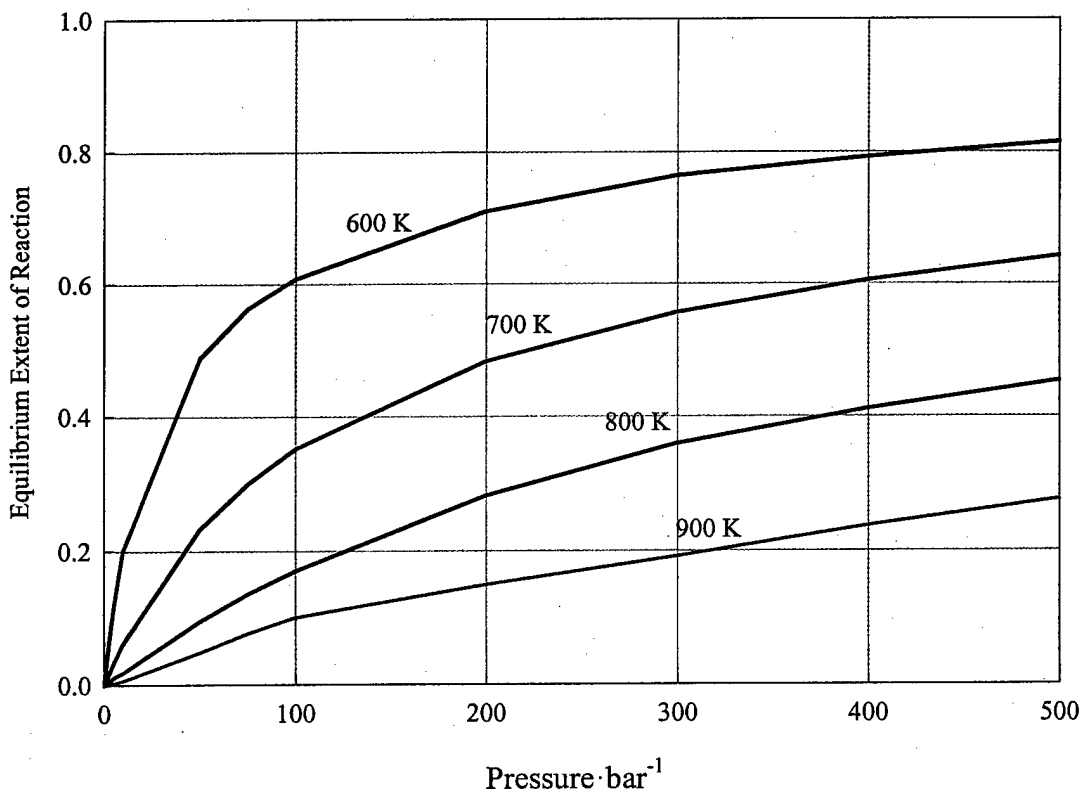

Figure 8. Equilibrium extent of reaction for the synthesis of ammonia from a stoichiometric mixture of hydrogen and nitrogen.

11. Kinetics of the Ammonia Synthesis

A fundamental problem for all reaction processes is the evaluation of the rate-determining step of a reaction pathway. This problem is of great importance since its solution reveals which step determines the rate of the whole reaction process. In the ammonia synthesis, however, there appears to be more than one rate-determining step.[4] If the ammonia synthesis reaction is considered to be homogeneous, it has an activation energy of approximately 230 kJ/mol of ammonia formed.[5] This large activation energy is several times larger than the corresponding Gibbs free energy change upon reaction and provides an explanation for the difficulty in obtaining ammonia within a reasonable period of time unless high temperatures are used and a low equilibrium extent of reaction is accepted. Thus, the use of a catalyst is necessary to obtain a sufficiently high reaction rate at a relatively low temperature.

One of the earliest and still very useful rate expressions developed for the ammonia synthesis is the Temkin-Pyzhev reaction rate equation. This rate expression was developed on the basis of chemisorption being quantitatively represented as a quasi-chemical reaction between a gas molecule A and an active center with mean activity l forming a monolayer on the surface:

$$A + l \rightleftarrows Al \tag{18}$$

Temkin and Pyzhev suggested that the chemisorption rate of this reaction is proportional to the partial pressure of species A only:

$$-\mathrm{d}p_A/\mathrm{d}t = k_f p_A \tag{19}$$

The desorption rate is considered to be independent of the partial pressure of A:

$$\mathrm{d}p_A/\mathrm{d}t = k'_f \tag{20}$$

Thus the total rate of reaction is the rate of adsorption less the rate of desorption:

$$r = k_f p_A - k'_f \tag{21}$$

The rate coefficients, k_f and k'_f, can be expressed as a function of temperature:

$$k_f = k \exp(-E_a/RT) \tag{22}$$

$$k'_f = k' \exp(-E_a'/RT) \tag{23}$$

In these expressions k and k' are frequency factors for the forward and reverse reactions (adsorption and desorption) and E_a and E_a' are the reaction activation energies. These two equations when substitued into equation 21 yield the following:

$$r = k p_A \exp(-E_a/\mathrm{RT}) - k' \exp(-E_a'/\mathrm{RT}) \tag{21}$$

Equations 22 and 23 are experimentally valid since the activation energy is sufficiently constant within a small temperature range in a quasi-chemical reaction such as chemisorption. This is a result of the rate constant's dependency on the chemisorption temperature. However, the activation energy also increases as the solid surface covered by the chemisorbed gas increases. Thus, it is safe to assume a linear relation between this activation energy and the concentration of the chemisorbed gas. As a result, the following approximations can be used:

$$E_a = a\, C_A \tag{25}$$

$$E_a' = b\, C_A \tag{26}$$

In these expressions a and b are empirical constants. Upon substitution of these expressions into equation 24, the following rate expression arises:

$$r = k p_A \exp(-a\, C_A/RT) - k' \exp(-b\, C_A/RT) \tag{27}$$

Temkin and Pyzhev viewed that the chemisorption of nitrogen was the rate determining step in which the following reaction occurs:

$$N_2 + 2l \rightleftarrows 2Nl \tag{28}$$

If in equation 27 $g = a/RT$ and $h = b/RT$ then the rate of nitrogen chemisorption is as follows:

$$r = k p_{N2} \exp(-g\, C_{N2}) - k' \exp(-h\, C_{N2}) \tag{29}$$

Temkin and Pyzhev abandoned the Langmuir adsorption concept which assumes the surface of the catalyst is energetically uniform. Instead, Temkin and Pyzhev used the Frumkin and Slygin adsorption equilibrium isotherm:

$$C_{N2} = (1/f) \ln(a_0 P_{N2}) \tag{30}$$

In this expression $f = g + h$ and $a_0 = k/k'$. Inserting this expression into equation 29 yields the following:

$$r = k p_{N2} \exp(-(g/f) \ln(a_0\, p_{N2})) - k' \exp(-(h/f) \ln(a_0\, p_{N2})) \tag{31}$$

Temkin and Pyzhev assumed that the amount of adsorbed nitrogen is determined by the equilibrium with hydrogen and ammonia in the gas phase. Thus, the nitrogen equilibrium pressure can be substitued into equation. The nitrogen equilibrium pressure is defined as follows:

$$p_{N2} = K_p p_{NH3}^2\, p_{H2}^{-3} \tag{32}$$

The resulting rate expression known as the Temkin-Pyzhev equation is as follows:

$$r = \kappa p_{N2} (p_{H2}^3/p_{NH3}^2)^{\alpha} - \kappa' (p_{NH3}^2/p_{H2}^3)^{1-\alpha} \tag{33}$$

The following lumped variable definitions are utilized in the Temkin-Pyzhev equation:

$$\alpha = g/f \tag{34}$$

$$\kappa = k(a_0 K_p)^{\alpha} \tag{35}$$

$$\kappa' = k'(a_0/K_p)^{1-\alpha} \tag{36}$$

In the Temkin-Pyzhev equation α, which relates the activation energy to adsorption heat, can be calculated from theoretical considerations and has a value in the range of 0.6 to 0.7.

12. Ammonia Synthesis Discussion

With the previous information pertaining to the synthesis of ammonia, one can quickly realize that the process is quite extensive and capital intensive. In addition the generation of syngas from hydrocarbons and subsequent shifting and purification are the same processes used to generate hydrogen from hydrocarbon-based fuels for PEM fuel cells. Thus, one may immediately argue that using ammonia decomposition processes to generate hydrogen is insensible. On a very large scale, on the order of a typical ammonia synthesis plant *i.e.* 1000 metric tons per day, ammonia synthesis followed by decomposition would almost never be performed. However, on a smaller scale, the decomposition of ammonia becomes attractive for generating hydrogen for PEM fuel cells. This attractiveness is based on the ease of the decomposition process and the lack of impurities such as sulfur and carbon oxides rather than the input requirements required to produce large-scale quantities of ammonia.

B. Ammonia Decomposition

The decomposition of ammonia can be performed readily via two distinct routes. The first route involves the thermal decomposition (cracking) of ammonia into nitrogen and hydrogen. The second route involves the autothermal decomposition of ammonia into nitrogen, hydrogen, and water. These pathways to hydrogen are schematically shown in figure 9.

1. Thermal Decomposition

The thermal decomposition of ammonia occurs via the following endothermic chemical reaction:

$$NH_3 \rightleftarrows 1/2\, N_2 + 3/2\, H_2 \qquad (\Delta H^0_{rxn} = 46\ kJ/mol) \tag{37}$$

As expected the thermal decomposition of ammonia is favored thermodynamically by high temperatures and low pressures. However, without the aid of a catalyst, this homogeneous decomposition rate is too low to be of any commercial importance. Heterogeneous ammonia decomposition rates have been shown to be greatly enhanced with the use of transition metals such as platinum either in the pure metallic state such as wires or supported as a dispersed metal on catalytic supports such as alumina.

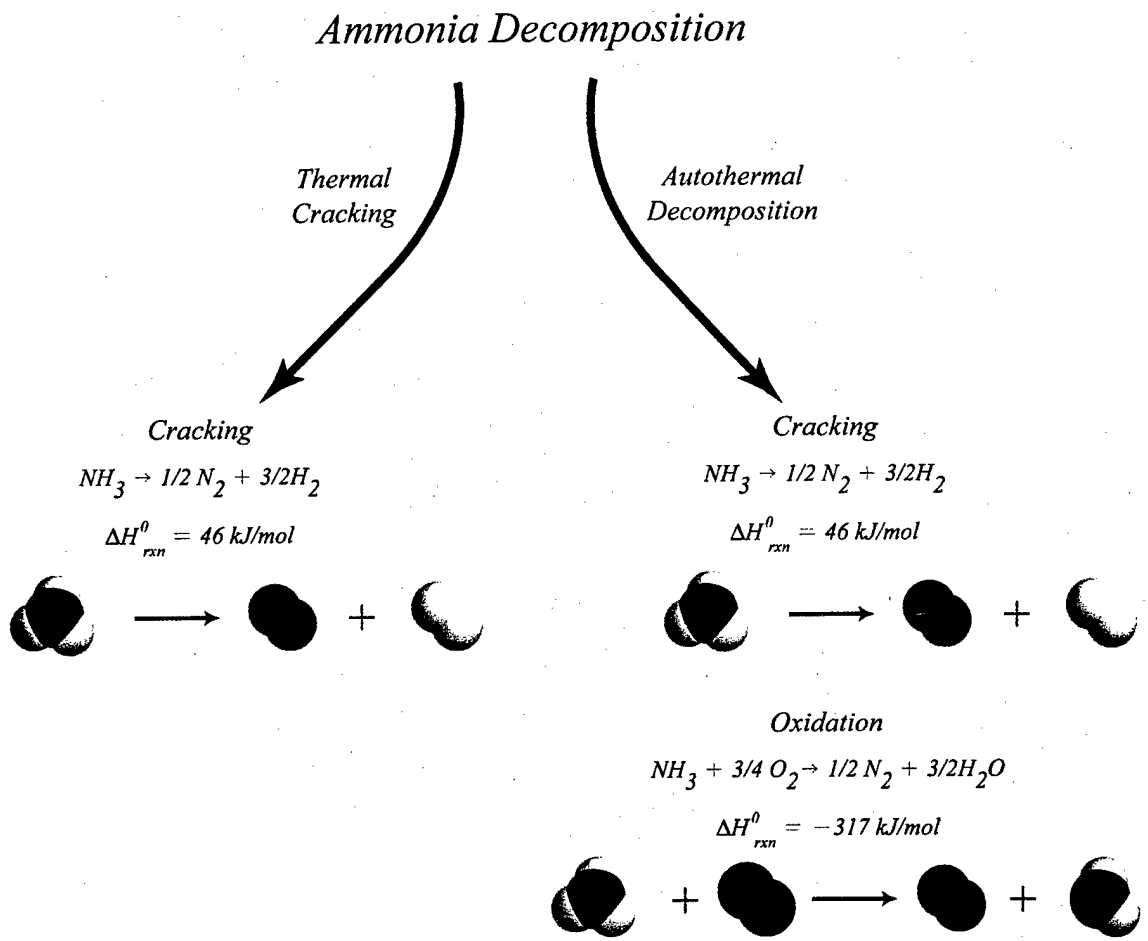

Figure 9. Two possible routes to hydrogen from ammonia.

Figure 10 plots the chemical equilibrium constant as a function temperature for the ammonia decomposition reaction as calculated with equation 17 and figure 11 plots the equilibrium extent of reaction at atmospheric pressure as a function of temperature as calculated with equation 16. For the calculations used to generate figure 11, the fugacity coefficient equilibrium ratio, K_v, in equation 16 is set to unity (ideal gas assumption). This assumption is valid since the decompostion favors low pressures.

The decomposition of ammonia with numerous transition metal catalysts has been studied extensively by various researchers.[6-9] Loffler *et. al* have shown that the rates of ammonia decomposition over a wide range of temperature and partial pressure can be fit to a Langmuir-Hinshelwood rate expression. At low temperatures the reaction rate is zeroeth order with respect to the partial pressure of ammonia. At higher temperatures the rate becomes dependent upon the partial pressure of ammonia. Indeed, the reaction rate becomes first order with respect to the partial pressure of ammonia.[7] The resulting Langmuir-Hinshelwood rate expression takes the following form:

$$r = k\,K_{NH3}\,p_{NH3} \,/\, (1 + K_{NH3}\,p_{NH3}) \tag{38}$$

In this expression k is the Arrhenius reaction rate constant and K_{NH3} is the ammonia adsorption

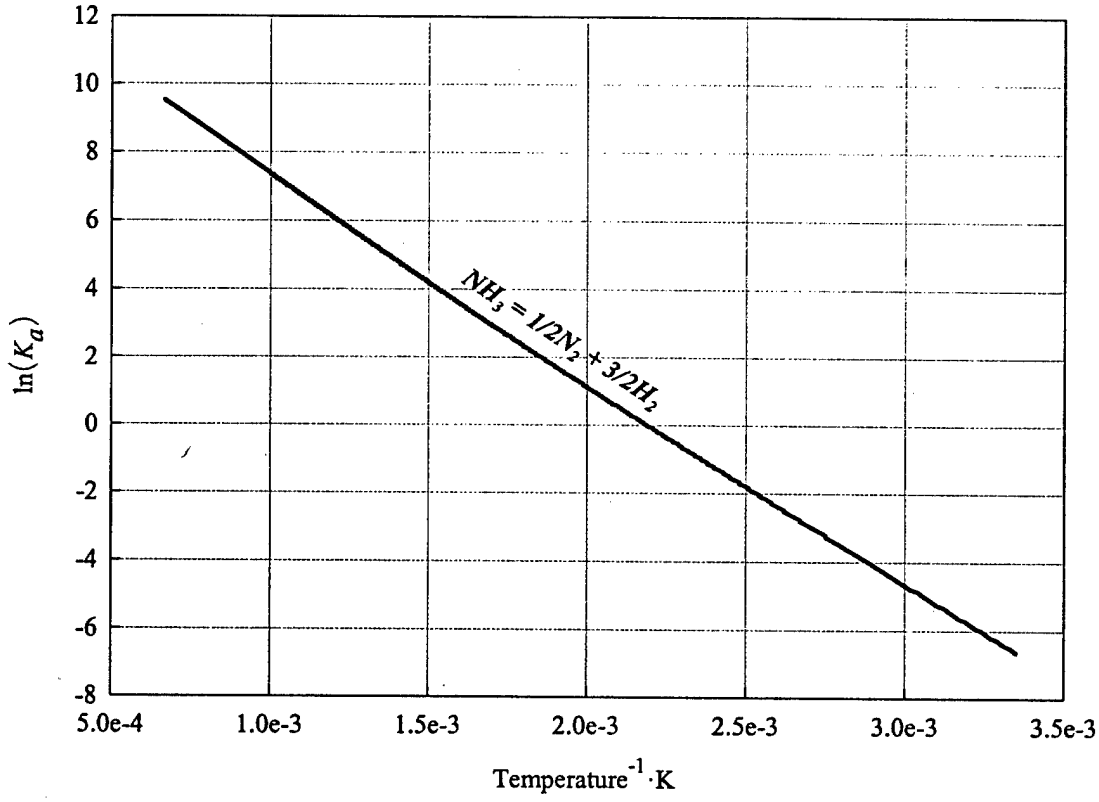

Figure 10. Chemical equilibrium constant for the decomposition of ammonia from pure ammonia as a function of temperature.

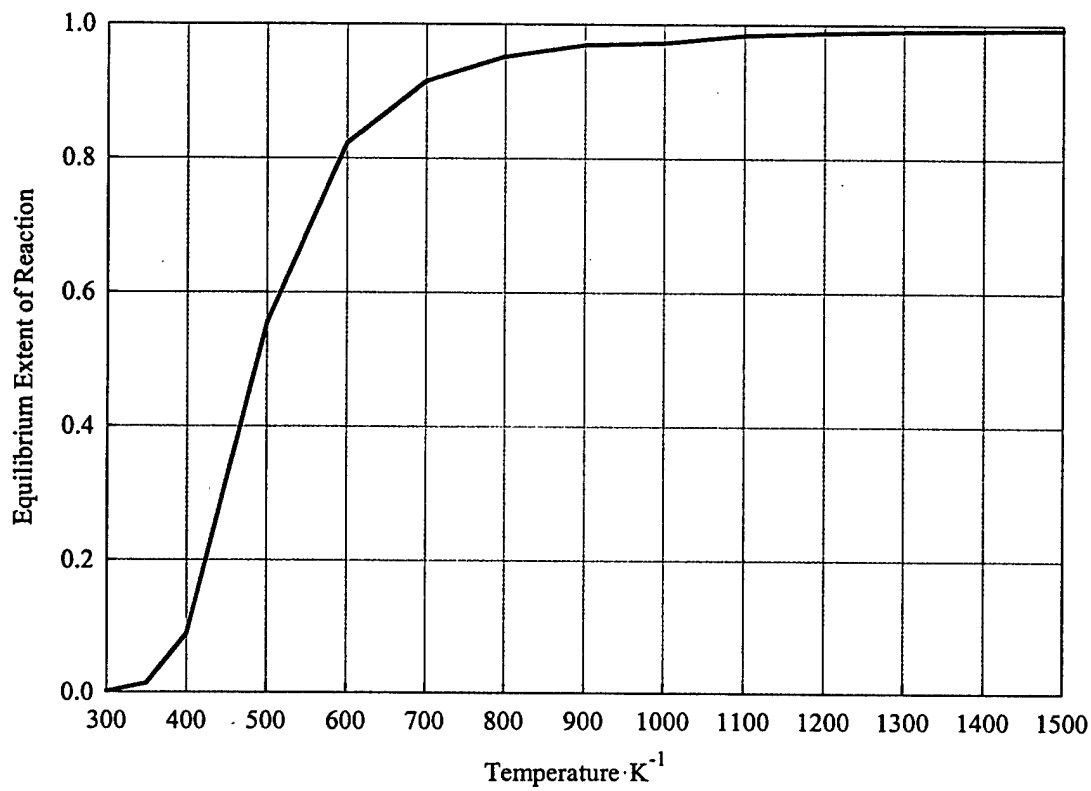

Figure 11. Equilibrium extent of reaction for the decomposition of pure ammonia.

constant usually expressed in Arrhenius form.

Aside from the Langmuir-Hinshelwood rate expression, Temkin and Pyzhev proposed a rate expression for the decomposition of ammonia based on the same assumptions used in formulating the rate expression for the ammonia synthesis. The Temkin-Pyzhev rate expression for the decomposition of ammonia is thus the desorption portion of the synthesis equation (equation 33):

$$r = -\mathrm{d}p_{NH3}/\mathrm{d}t = \kappa'\left(p^2_{NH3}/p^3_{H2}\right)^{1-\alpha} \tag{39}$$

Love and Emmett[10] verified the Temkin-Pyzhev rate expression for the decomposition of ammonia over both singly and doubly promoted promoted catalysts at atmospheric pressure and arrived at the following expression:

$$r = -\mathrm{d}p_{NH3}/\mathrm{d}t = \kappa'\left(p^{0.58}{}_{NH3}/p^{0.87}{}_{H2}\right) \tag{40}$$

This expression is identical to the Temkin-Pyzhev equation with α equal to 0.29. In addition the apparent activation energy for decomposition was found to be 190 ± 8 kJ/mol

2. Autothermal Decomposition

Although ammonia decomposition can be performed via thermal cracking at modest rates, a significant amount of energy must be put into the reaction system to get hydrogen out. An alternative to this route to hydrogen is the autothermal ammonia decomposition over a transition metal catalyst. Hydrogen generation via this route is obtained by reacting ammonia and oxygen (or air) autothermally in which a portion of the ammonia is combusted to deliver heat to the endothermic cracking of ammonia. Thus, two primary reactions occur simultaneously in the same reaction zone:

$$NH_3 + 3/4O_2 \rightarrow 1/2\,N_2 + 3/2\,H_2O \qquad \left(\Delta H^0_{rxn} = -317\ kJ/mol\right) \tag{41}$$

$$NH_3 \rightleftarrows 1/2\,N_2 + 3/2\,H_2 \qquad \left(\Delta H^0_{rxn} = 46\ kJ/mol\right) \tag{42}$$

An immediate advantage of this route to hydrogen is that the reaction system can be thermally self-sustaining upon ignition. A disadvantage of this system is a certain amount of ammonia is lost to nitrogen and water thus reducing the overall hydrogen-content of the system. However, the amount of ammonia oxidized can be tailored by changing the ammonia:oxygen ratio in the feed since in this combustion process the oxygen is the limiting reagent. Ideally, adiabatic operation of the reaction system is desired since larger ammonia:oxygen ratios can be used minimizing the amount of ammonia oxidized. Figure 12 plots the adiabatic flame temperature of ammonia in air at various ammonia:oxygen ratios. From figure 12 it can be seen that temperatures in excess of 1000 K can be achieved with room temperature feed at ammonia:oxygen ratios as large as 10.

Heterogeneous thermal decomposition of ammonia has already been discussed in detail and can be considered to be one of the reactions occuring in the autothermal ammonia decomposition. However, in the autothermal process, there is an additional reaction, the oxidation of ammonia, that is coupled to the thermal decomposition reaction. As in thermal decompotion, the oxidation of ammonia can occur either as a homogeneous gas phase reaction or on a solid surface as a heterogeneously catalyzed reaction. The heterogeneous oxidation of ammonia over platinum, rhodium, and palladium has been studied

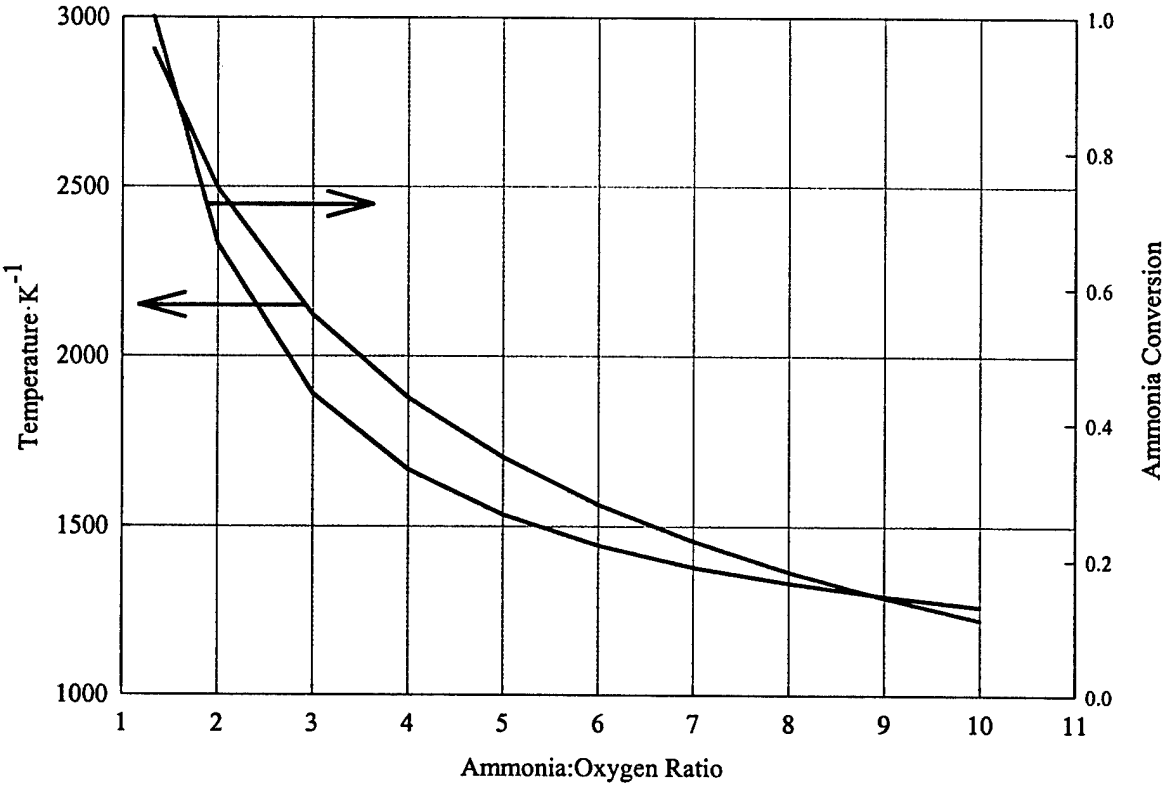

Figure 12. Adiabatic flame temperature and ammonia conversion for ammonia/air mixtures fed at 25°C with complete oxygen consumption.

extensively by Schmidt *et. al.*[11-13]

Whenever nitrogen-containing species are combusted, the formation of nitric oxide and nitrogen dioxide must be carefully examined. A thermodynamic examination of the chemical equilibrium constants for the formation of nitrogen oxide compounds is useful here since it provides insight into the conditions that favor or disfavor formation. Figure 13 plots the chemical equilibrium constants at atmospheric pressure as a function of temperature for a number of ammonia decomposition reactions as well as the formation of nitrogen oxide and nitrogen dioxide:

$$1/2\ O_2 + 1/2\ N_2 \rightleftarrows NO \qquad (\Delta H^0_{rxn} = 90.37\ kJ/mol) \qquad (43)$$

$$NO + 1/2\ O_2 \rightleftarrows NO_2 \qquad (\Delta H^0_{rxn} = -56.57\ kJ/mol) \qquad (44)$$

Figure 14 reveals that from a thermodynamic point-of-view the incorporation of oxygen into water through reaction with ammonia is much more favorable than oxygen incorporation into nitric oxide or nitrogen dioxide.

In an autothermal reaction system a source of heat from an exothermic reaction is required to drive an endothermic reaction. In this reaction system the source of heat is the combustion of ammonia. At low ammonia:oxygen ratios a large portion of ammonia is combusted with the large amount of oxygen present (reacting oxygen to completion). If the reaction system operates adiabatically or as the reaction

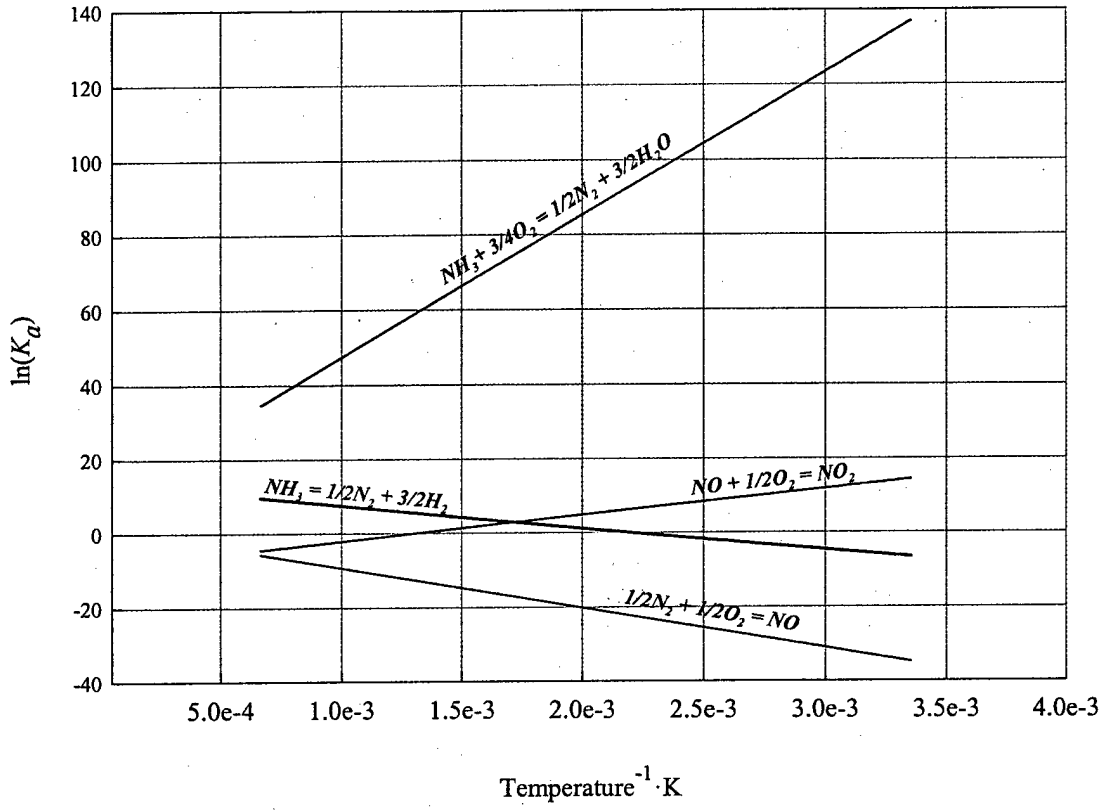

Figure 13. Chemical equilibrium constant for the decomposition of ammonia and the formation of nitrogen oxides as a function of temperature.

system approaches adiabatic operation, the ammonia:oxygen ratio can be increased so that less ammonia is needed for the combustion reaction. This is desired so that the efficiency of the system can be improved *i.e.* more hydrogen is incorporated into diatomic hydrogen instead of water. At this point the design of the chemical reactor becomes the most important factor in improving the efficieny of the reaction system.

The basic goal of designing an autothermal ammonia decomposition reaction system is to keep as much heat inside the system as possible *i.e.* strive toward adiabaticity. Heat losses through radiation, conduction, and convection must thus be minimized. Radiative losses are important here since the reaction system operates at high temperatures and radiative heat transfer rates are proportional to absolute temperature raised to the fourth power. Visually, the reaction zone in the ammonia decomposition system appears bright orange indicating immediately that radiative heat transfer is occurring. Figure 14 is a picture of an uninsulated autothermal ammonia decomposition reaction system revealing that radiative heat transfer is present.

Radiative heat transfer is quantified through the following equation:

$$q_{rad} = A\varepsilon\sigma T^4 \tag{45}$$

In this equation q_{rad} is the heat transfer rate in Watts, ε is the body emissivity, σ is a constant, and T is the absolute temperature of the body. Thus, to minimize radiative heat losses one would immediately want to reduce the operating temperature since the heat loss is proportional to T^4. This can be achieved

by operating at larger ammonia:oxygen ratios since this reduces the adiabatic flame temperature (see Figure 12).

Figure 14. Autothermal ammonia decomposition conducted in an experimental quartz reactor.

The tailoring of the emissivity depends upon the location in the reaction system. In the interior of the reactor, low emmisivity materials should be used. However, once radiation leaves the interior of the reactor, it is desired to return the radiation towards the interior. In this case large emissivity materials are desired to improve radiative heat transfer back into the reaction system.

Conductive and convective heat treansfer is expressed as follows:

$$q_{cond,x}/A = -k\,\mathrm{d}T/\mathrm{d}x \tag{46}$$

$$q_{conv} = hA(T_w - T_f) \tag{47}$$

In these equations q is the heat tranfer rate in Watts, A is the area, k is the thermal conductivity, x is the direction of heat transfer, h is a heat transfer coefficient, T_w is the temperature of the solid surface, and T_f is the temperature of the fluid flowing past the surface.

Once again, in order to keep as much of the thermal energy inside the reaction system, conductive and convective heat losses to the exterior must be minimized. However, conductive and convective heat transfer is desired to transfer heat from the hot effluent leaving the reactor to the gas stream feeding the reactor.

Two important reactor configurations were used to study the autothermal ammonia decomposition. The first reactor configuration, the single-pass straight-tube reactor, has a very simple geometry and does not utilize heat transfer from the reactor effluent to the reactor feed. The second reactor configuration, the two-pass coaxial reactor utilizes a feed preheat via heat transfer from the reactor effluent. These reactor configurations are shown in figure 15 and figure 16. Also indicated in this figure is the catalyst bed in the form of a foam monolith containing a deposited metal. Located on both sides of the catalytic monolith is another monolith containing no catalyst. The purpose of these monoliths is to reduce radiative heat losses.

The last item of discussion pertaining to the autothermal ammonia decomposition is to lay out the working equations that define the feed gas and reactor performance. The equations shown in table 3 define the composition, volumetric flow rate, and molar flow of the feed gas in terms of the ammonia:oxygen ratio and total volumetric feed rate. These equations are based on air providing the

oxygen. Table 4 provides the definitions of ammonia conversion, selectivity to hydrogen, and selectivity to water. This table also provides equations for the effluent molar flow rates in terms of the ammonia molar feed rate, ammonia conversion, and selectivity to hydrogen. In addition, equations defining the extent of reactions are provided.

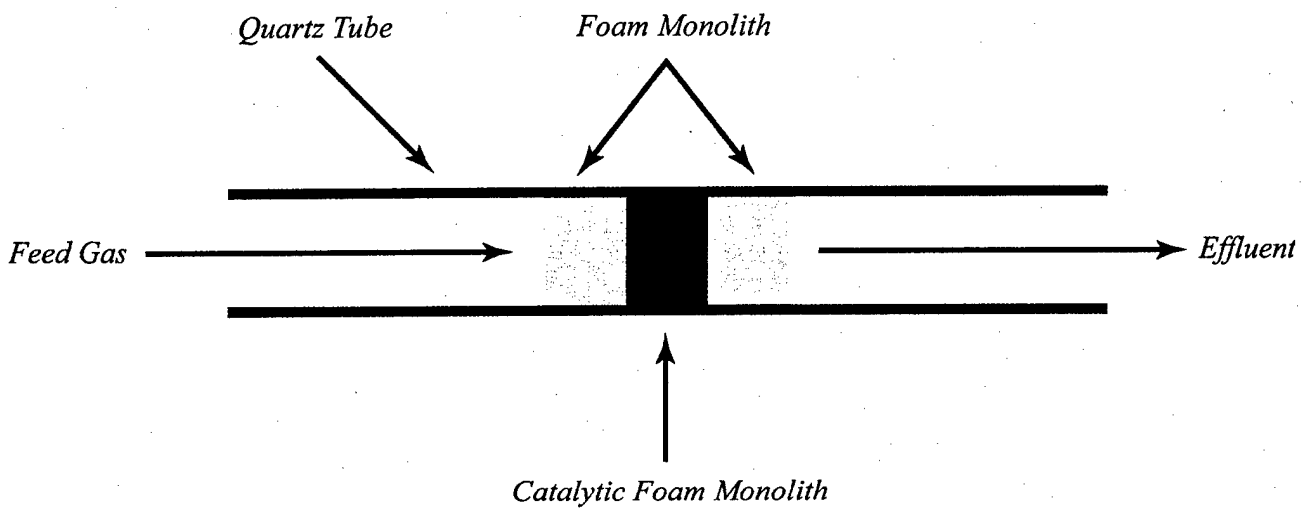

Figure 15. Experimental single-pass straight-tube reactor for the autothermal ammonia decomposition.

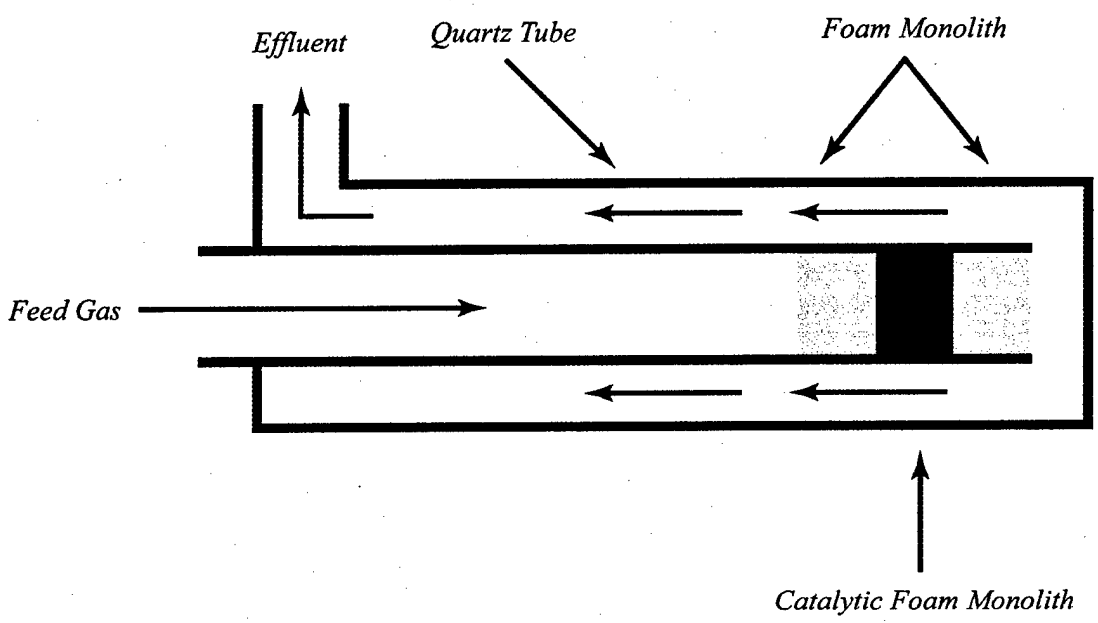

Figure 16. Experimental two-pass coaxial reactor for the autothermal ammonia decomposition.

Table 3. Feed Gas Equations

$\Phi = NH_3{:}O_2$ *Ratio*

V_0 = *Total volumetric flow rate*

$y_{i,0}$ = *Mole fraction of species i*

$n_{i,0}$ = *Molar flow rate of species i*

ζ = *Conversion factor*

$$y_{NH_3,0} = \frac{\Phi}{\Phi + 4.76} \quad (48)$$

$$y_{N_2,0} = \frac{3.76}{\Phi + 4.76} \quad (49)$$

$$y_{O_2,0} = \frac{1}{\Phi + 4.76} \quad (50)$$

$$y_{air,0} = \frac{4.76}{\Phi + 4.76} \quad (51)$$

$$V_{NH_3,0} = \frac{V_0 \Phi}{\Phi + 4.76} \quad (52)$$

$$V_{N_2,0} = \frac{V_0\, 3.76}{\Phi + 4.76} \quad (53)$$

$$V_{O_2,0} = \frac{V_0}{\Phi + 4.76} \quad (54)$$

$$V_{air,0} = \frac{V_0\, 4.76}{\Phi + 4.76} \quad (55)$$

$$n_{NH_3,0} = \zeta \frac{V_0 \Phi}{\Phi + 4.76} \quad (56)$$

$$n_{N_2,0} = \zeta \frac{V_0 3.76}{\Phi + 4.76} \quad (57)$$

$$n_{O_2,0} = \zeta \frac{V_0}{\Phi + 4.76} \quad (58)$$

$$n_{air,0} = \zeta \frac{V_0 4.76}{\Phi + 4.76} \quad (59)$$

$$\zeta = 4.1411 \times 10^{-5} \text{ mol/cm for } V_0 \text{ in sccm} \quad (60)$$

$$\zeta = 4.1411 \times 10^{-2} \text{ mol/l for } V_0 \text{ in slpm} \quad (61)$$

Table 4. Reactor Performance Equations

X_{NH_3} = *Conversion of ammonia*

S_i = *Selectivity to species i*

ξ_i = *Extent of reaction i*

$n_{i,0}$ = *Feed molar flow rate of species i*

n_i = *Exit molar flow rate of species i*

Reaction 1 $NH_3 \rightarrow 1/2N_2 + 3/2H_2$ (62)

Reaction 2 $NH_3 + 3/4O_2 \rightarrow 1/2N_2 + 3/2H_2O$ (63)

$$X_{NH_3} = \frac{n_{NH_3,0} - n_{NH_3}}{n_{NH_3,0}} \quad (64)$$

$$S_{H_2} = \frac{n_{H_2} - n_{H_2,0}}{n_{H_2} - n_{H_2,0} + n_{H_2O} - n_{H_2O,0}} \quad (65)$$

$$S_{H_2O} = 1 - S_{H_2} \quad (66)$$

$$\xi_1 = S_{H_2} X_{NH_3} n_{NH_3,0} \quad (67)$$

$$\xi_2 = S_{H_2O} X_{NH_3} n_{NH_3,0} \quad (68)$$

$$n_{NH_3} = (1 - X_{NH_3}) n_{NH_3,0} \quad (69)$$

$$n_{O_2} = n_{O_2,0} - 3/4(1 - S_{H_2}) X_{NH_3} n_{NH_3,0} \quad (70)$$

$$n_{N_2} = n_{N_2,0} + 1/2 X_{NH_3} n_{NH_3,0} \quad (71)$$

$$n_{H_2} = n_{H_2,0} + 3/2(1 - S_{H_2}) X_{NH_3} n_{NH_3,0} \quad (72)$$

$$n_{H_2O} = n_{H_2O,0} + 3/2(1 - S_{H_2}) X_{NH_3} n_{NH_3,0} \quad (73)$$

C. Ammonia Adsorption

It has been mentioned that the adsorption of ammonia onto a substrate such as a zeolite or activated charcoal is important for removing residual amounts of ammonia from the autothermal ammonia decomposition reactor effluent stream. Adsorption processes can also be important for the protection of an anhydrous ammonia storage vessel where the substrate can act as barrier to prevent the release of ammonia to the surroundings. Of course the amount of ammonia contacting the substrate variers over several orders of magnitude when going from simple effluent polishing to storage vessel protection. Nonetheless, a discussion concerning the adsorption of a gas onto a solid is important for understanding ammonia adsorption.

1. Chemisorption and Physisorption

Adsorption on solids (adsorbents) can be classified into two catergories: physical adsorption (physisorption) and chemical adsorption (chemisorption). In physical adsorption gas molecules (adsorbate) are held to the solid's surface by relatively weak intermolecular van der Waals forces, where as in chemical adsorption a chemical reaction occurs at the solid's surface where the gas molecules are held by relatively strong chemical bonds. In a more general sense, physisorption is nonspecific i.e. nitrogen will adsorb onto virtually any solid surface if the temperature is low enough, and chemisorption is highly specific in that it is similar to ordinary chemical reactions.

The differences between chemisorption and physisorption can also be related to enthalpy changes in that the enthalpy changes for chemisorption are usually greater in magnitude than those for physisorption. Enthalpy changes for chemisorption processes typically fall in the range of -40 to -800 kJ mol^{-1}. On the other hand, enthalpy changes for physisorption typically fall in the range of -4 to -40 kJ mol^{-1} *i.e.* similar to the enthalpy change associated with the condensation of a gas. In chemisorption chemical bonds may be broken as well as formed. As a result enthalpy changes during chemisorption can be positive or negative. However, the entropy change during chemisorption will be quite negative since the species being adsorbed enter or much more ordered state. As a result, the enthalpy change associated with chemisorption must be quite negative in order to produce any significant amount of adsorption.

Once a monolayer of adsorbed gas covers a solid's surface during chemisorption, no further chemical reaction can occur between the gaseous species and the solid. However, in physisorption, once a monolayer is formed, intermolecular interactions between the adsorbed species in the monolayer and gaseous species can lead to the formation of a second layer of adsorbed species. Indeed, the enthalpy change associated with the formation of the first physisorbed layer is determined by gas-solid interactions, whereas the formation of subsequent layers is determined by gas-gas interactions and have enthalpy changes similar to that of the species condensing from the gas to liquid phase.

The adsorption of ammonia primarily occurs via chemisorption and is similar to the adsorption of carbon monoxide and ethylene. Since species such as ammonia, carbon monoxide, and ethylene have unshared electron pairs or multiple bonds chemisorption can occur without dissociating (nondissociative or molecular adsorption). On the other hand, species such as hydrogen and methane usually dissociate during the chemisorption process (dissociative adsorption).

2. Adsorption Isotherms

Under ordinary conditions, the surface of any solid is covered with adsorbed species derived mainly from the atmosphere. Thus, in order to conduct a gas-solid adsorption study the solid's surface must be cleaned. This is usually accomplished through the heating of the solid under vacuum in a procedure termed *outgassing*. An alternative procedure is to vaporize the solid in a vacuum followed by condensation into a thin film on another solid surface. After the surface of a solid has been cleaned, an adsorption study can proceed. This is usually accomplished by measuring the amount of gas adsorbed at a given temperature as a function of gas pressure in equilibrium with the solid. Thus, by repeating the experiment with different initial pressures of gas one can gather data for the amount of adsorbed species as a function of equilibrium gas pressure at a fixed adsorbent temperature. Finally, an adsorption isotherm can be generated by plotting the moles of gas adsorbed per mass of adsorbent versus equilibrium gas pressure at a fixed temperature. It has been traditional to plot adsorption isotherms with the amount adsorbed expressed in terms of the gas volume (corrected to 0°C and 1 atm) adsorbed per gram of adsorbent. Figure 17 shows a typical adsorption isotherm.

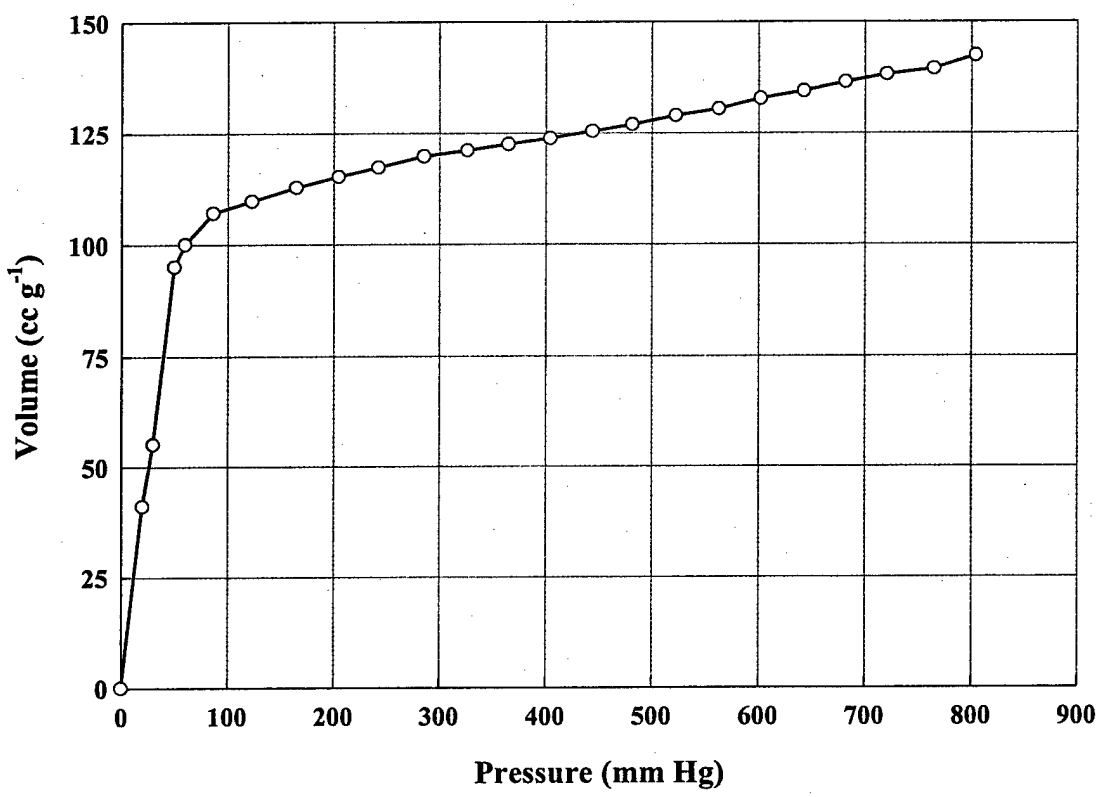

Figure 17. Adsorption isotherm for ammonia on a zeolite at 25°C.

In 1918 Langmuir used a simple model of a solid surface to derive an equation for an adsorption isotherm. He made a number of assumptions which included: a uniform solid surface, adsorbed molecules do not interact with one another, adsorbed molecules are localized at specific sites, and only a monolayer can adsorb. Now, at equilibrium the rate of adsorption to the surface equals the rate of desorption from the surface. If N equals the number of available adsorption sites on the bare solid surface and θ is the fraction of adsorption sites occupied by the adsorbate at equilibrium, then the rate of desorption is proportional to the number of adsorbed molecules (θN) and is equal to $k_d \theta N$, where k_d is a constant at fixed temperature. The adsorption rate is proportional to the rate of gas-phase collisions with unoccupied adsorption sites (only a monolayer is assumed to form). Thus, the rate of collisions of gas molecules with the surface is proportional to the gas pressure P and the number of unoccupied sites $(1-\theta)N$. Therefore, the adsorption rate is $k_a P(1-\theta)N$, where k_a is a constant at fixed temperature. If we equate the rates of adsorption and desorption the following results:

$$k_a P(1-\theta)N = k_d \theta N \tag{74}$$

Substituting $b(T) \equiv k_a / k_d$ into equation 74 and solving for θ results in the following:

$$\theta = bP/(1+bP) \tag{75}$$

Since the rate constants depend upon temperature, b also depends upon temperature. In addition, the fraction of sites (θ) occupied at pressure P is equal to υ/υ_{mon}, where υ is the volume adsorbed (corrected to 0°C and 1 atm) at pressure P, and υ_{mon} is the volume adsorbed (corrected to 0°C and 1 atm) in the high pressure limit when a monolayer covers the entire surface. Thus, equation 75 becomes as follows:

$$\upsilon = \upsilon_{mon} bP/(1+bP) \tag{76}$$

Equation 76 is known as the Langmuir isotherm. In the low pressure limit the denominator in equation 76 can be neglected and θ increases linearly with pressure. In the high-pressure limit θ approaches unity.

Although most of Langmuir's assumptions are false, his derivation provides insight into the adsorption process. Many other researchers have dedicated much of their lives studying the adsorption process and have developed more complex models of the adsorption process.

D. Ammonia Storage

The materials of construction for equipment to transport and store ammonia are largely dictated by the amount of water present in the ammonia. If ammonia is free of moisture (anhydrous) virtually any metal can be used. However, the presence of moisture and/or the presence of trace amounts of oxygen and carbon dioxide greatly increases the corrosiveness of ammonia.

Commercially, anhydrous ammonia (liquid) is sold in tankers or cylinders made of carbon steel. Storage vessels for anhydrous ammonia are also usually constructed of carbon steel whereas vessels storing aqueous ammonia are typically constructed of 316 stainless steel. Vessels containing anhydrous ammonia are usually filled to a capacity of 0.53 kg liter^{-1}; the vessels are tested hydraulically to a pressure of 34 kg cm^{-2}. Vessels containing aqueous ammonia are usually filled to a capacity of 0.80 kg liter^{-1}; the vessels are tested hydraulically at 11 kg cm^{-2} for a 35 wt% ammonia solution.

With respect to this project, small quantities of ammonia (on the order of a few hundred grams) need to be stored. An obvious material of choice for the storage of ammonia is aluminum. Aluminum is compatible with anhydrous ammonia and exhibits great properties; aluminum is lightweight, strong, and inexpensive. Ammonia storage in aluminum canisters will be further discussed later in this report.

E. PEM Fuel Cells

As previously indicated, one use for the autothermal ammonia decomposition reactor is to provide hydrogen for a hydrogen/air PEM fuel cell. The following section discusses briefly the basic theory behind fuel cell operation.

1. Fuel Cell Operation

Very simply, a fuel cell is a device that converts chemical energy into electrical energy through the electrochemical reaction of a fuel (in this case hydrogen) with oxygen (obtained from air). The electrochemistry that occurs can be divided into two parts (half-cell reactions) that occur on separate electrodes. Half-cell reactions occur in pairs in which oxidation occurs at the anode and reduction occurs at the cathode. Thus, the reaction at the cathode consumes the electrons produced at the anode. For the case of a hydrogen/oxygen PEM fuel cell the following half cell reactions occur:

$$H_2\,(g) \rightarrow 2\,H^+\,(aq) \;+ 2\,e^- \tag{77}$$

$$1/2O_2\,(g) + 2\,H^+\,(aq) \;+ 2\,e^- \rightarrow H_2O\,(l) \tag{78}$$

If equations 77 and 78 are combined, the overall cell reaction is as follows:

$$H_2\,(g) + 1/2O_2\,(g) \rightarrow H_2O\,(l) \tag{79}$$

To facilitate each half-cell reaction, porous electrodes must contain an electro-catalyst. This electro-

catalyst is usually platinum based and increases the rates for the thermodynamically favored reactions. When the reactions occur, protons (hydrogen ions) and electrons produced at the anode from hydrogen (fuel) travel separate paths to recombine at the cathode where the oxygen is reduced. It is important to note that an electrolyte is needed to allow ions to travel so that the overall condition of the cell is one of electro-neutral *i.e.* zero net charge, electronic or ionic.

In a PEM fuel cell a solid polymer electrolyte is employed. A common solid polymer electrolyte is Nafion which is an acidic solid polymer electrolyte. Acidic polymer electrolytes are electrically insulating, polymeric membranes selective for proton transfer via acid groups attached to the hydro- or fluoro-carbon polymer backbone. The acid groups of these electrolytes are typically protonated anions such as sulfonic acid bonded to a polymer side chain. The structurally immobile acid groups allow only cations or neutral species to enter the membrane. Also, since the acid groups are immobile concentration gradients inside the electrolyte are prevented.

In order to maximize the power density of a fuel cell, electrode structures must be fabricated in such a way that the area where reactions occur is large. The active area is thus maximized through the use of porous electrodes. Although the reactions may occur at a relatively small current density, the high internal surface area of a porous electrode allows for the production of a large current in a small volume. These porous electrodes are generally fabricated from a composite network of small catalyst particles (10 - 50 nm). Typically, a portion of the pore space in the network of catalyst particles is filled with electrolyte. Finally, when a catalyzed porous electrode is placed on both sides of a solid polymer electrolyte membrane followed by a porous current collector a PEM fuel cell results.

It is important to note that in order for a catalyst particle in the porous electrode to be active, it must have contact with at least four different phases simultaneously: electrons produced or consumed on a particle must have a continuous electronic pathway to or from the current collector, the protons produced or consumed on the particle must have a conductive path through an ionic conducting phase to the polymer electrolyte membrane, reaction products must be able to reach the particle, and products must be able to leave the particle.[11]

2. Fuel Cell Thermodynamics

Thermodynamic analysis of fuel cell systems is useful in predicting the maximum possible fuel cell potential for a given fuel and its maximum overall efficiency. One must remember, however, that thermodynamics can yield no information concerning the rate of energy production.

Assuming that only fuel oxidation occurs at the anode and oxygen reduction occurs at the cathode, then at open circuit conditions (zero current flow between the electrodes) an open circuit potential can be measured between the two electrodes. If it is further assumed that electrode reactions are reversible and that all reactants are at standard conditions (1 bar and 25°C) with activities of unity, then this open circuit potential will be the standard cell potential. The standard cell potential (E^0_{cell}) is a measure of the maximum free energy change that can occur and can be calculated using the following equation:

$$E^0_{cell} = -\Delta G^0_{rxn} / nF \qquad (80)$$

In equation 80 n is the number of electrons per molecule oxidized or reduced and F is Faraday's constant, 96485 C (mole e^-)$^{-1}$.

If the reactants are not at standard conditions and their activities are not unity, the cell potential

(E_{cell}) can be calculated with a similar equation as follows:

$$E_{cell} = -\Delta G_{rxn} / nF \tag{81}$$

Equation 81 is useful when a fuel cell is operating because the free energy change can be calculated from a measured cell potential.

Aside from the standard cell potential, the standard free energy change can also be used to calculate the standard specific energy for a fuel (φ^0_{fuel}) as follows:

$$\varphi^0_{fuel} = |277.8 \cdot \Delta G^0_{rxn} / MW_{fuel}| \tag{82}$$

In equation 82 MW_{fuel} is the molecular weight of the fuel.

Up until now, the free energy change of reaction has been used. The free energy change of reaction (ΔG^0_{rxn}) is the fraction of the total energy change that can be used to do work (converted into electrical energy). The enthalpy change of reaction (ΔH^0_{rxn}), on the other hand, defines the total amount of energy released during the reaction. The ratio of these quantities is used to define the thermodynamic efficiency of an electrochemical reaction. The thermodynamic efficiency is thus defined as:

$$\varepsilon_t = 100 \cdot \Delta G^0_{rxn} / \Delta H^0_{rxn} \tag{83}$$

Table 5 lists various thermodynamic quantities for the hydrogen/oxygen electrochemical reaction. As shown in table 5 a thermodynamic efficiency of 100% is not achieved; the difference between the enthalpic and free energy change is lost entropically. Note, too, that an actual fuel cell will operate with

Table 5. Thermodynamic Analysis of H_2/O_2 Electrochemical Cell

Reaction	$H_2\,(g) + 1/2O_2\,(g) \rightarrow H_2O\,(l)$
n	2
ΔG^0_{rxn}	-237 kJ mol^{-1}
E^0_{cell}	1.229 V
φ^0	32700 Wh kg^{-1}
ΔH^0_{rxn}	-286 kJ mol^{-1}
ε_t	83.0 %

efficiencies less than the thermodynamic efficiency calculated using equation 82 because kinetics prevents standard potentials from being achieved.

Next, the overall fuel cell efficiency (ε_{tot}) can be calculated through the use of voltage (ε_v) and current (ε_I) efficiencies along with the thermodynamic efficiency of the electrochemical reaction. Voltage efficiency accounts for the kinetic and ohmic potential losses (overpotentials) which cause the cell potential to be reduced from the standard cell potential during fuel cell operation. Kinetic overpotential is due to the irreversibilities present in fuel cell operation. Ohmic overpotential is caused by ionic and electronic resistance to current flow inherent in the fuel cell. Finally, voltage efficiency can be expressed as follows:

$$\varepsilon_v = 100 \cdot E_{cell} / E^0_{cell} \tag{84}$$

Current efficiency (fuel utilization) arises from side reactions and other losses of fuel which do not contribute to the measured fuel cell current (I_{cell}). Essentially, current efficiency is the ratio of the fuel consumed in producing current to the total amount of fuel consumed. Loss current (I_{loss}) is the sum of all sources of fuel consumption (aside from the desired electrochemical reaction) converted to oxidation current as if the fuel had been reacted on the anode. Current efficiency is thus defined as follows:

$$\varepsilon_I = 100 \cdot I_{cell} / (I_{cell} + I_{loss}) \tag{85}$$

Finally, the overall fuel cell efficiency can be calculated with the following equation:

$$\varepsilon_{tot} = 1 \times 10^{-4} \cdot (\varepsilon_v \, \varepsilon_I \, \varepsilon_t) \tag{86}$$

Typical values for the overall fuel cell efficiency run between 20% and 50%.[12] A hydrogen/oxygen PEM fuel cell typically has an overall efficiency closer to 50% due to more effective electrocatalysis and a current efficiency approaching 100%.

III. EXPERIMENTAL

A hydrogen-generating catalytic reactor based on the autothermal decomposition of ammonia and coupled to a PEM fuel cell has been experimentally studied on the laboratory scale. All of the necessary materials and equipment used to conduct the research are described in this section. In addition, the experimental procedures are outlined.

A. Materials

The primary use of materials in this project was for the generation of catalysts. Four different supported catalysts and one pure metallic catalyst were studied; the supported catalysts used either an alumina foam monolithic support or an alumina sphere support. The feed gases used in this research consisted of ammonia, air, and argon. These research-grade gases were supplied to the hydrogen-generating catalytic reactor from standard gas cylinders through mass flow controllers. Lastly, a zeolite bed was used to polish the reactor effluent before it was fed to the fuel cell.

1. Catalyst Metals

A variety of supported catalysts were prepared and tested in the hydrogen-generating catalytic reactor. In order to prepare the supported metal catalysts, metal salt solutions were purchased. Table 7 lists information for these metals.

Table 6. Metal Salt Solutions Used for Supported Catalyst Preparation

Metal	Initial Form	Solvent
Ruthenium	$RuCl_3 \cdot 3H_2O$	Water
Nickel	$Ni(NO_3)_2 \cdot 6H_2O$	Water

In addition to the aforementioned supported catalysts used in this research, a 40 mesh woven nickel gauze was also used as a catalyst; the gauze was simply cut into 4.75 mm diameter disks and used in the pure metallic state.

2. Catalyst Support

Foam monolithic catalyst supports were purchased from Vesuvius-McDanel. These supports consisted of α-Al_2O_3 with a surface area of approximately 0.10 $m^2 g^{-1}$ and a macroscopic porosity of 80

pores per inch. A high pressure fluid jet was used to cut 4.75 mm diameter monoliths from 20 mm diameter monoliths. The depth of both monoliths was 10 mm. In addition to using monolithic supports, α-Al_2O_3 spheres with a diameter of 1 mm were also tested. These spheres has an approximate surface area of 120 $m^2 g^{-1}$.

3. Feed Gas

Research-grade ammonia and argon were dispensed from standard gas cylinders. The argon was passed through molecular sieve beds to remove impurities. The ammonia is stored in a cylinder as a liquid under its own vapor pressure which is approximately 129 psia. Since ammonia is the most important feed to the reactor system, its vapor pressure curve is shown in figure 18.

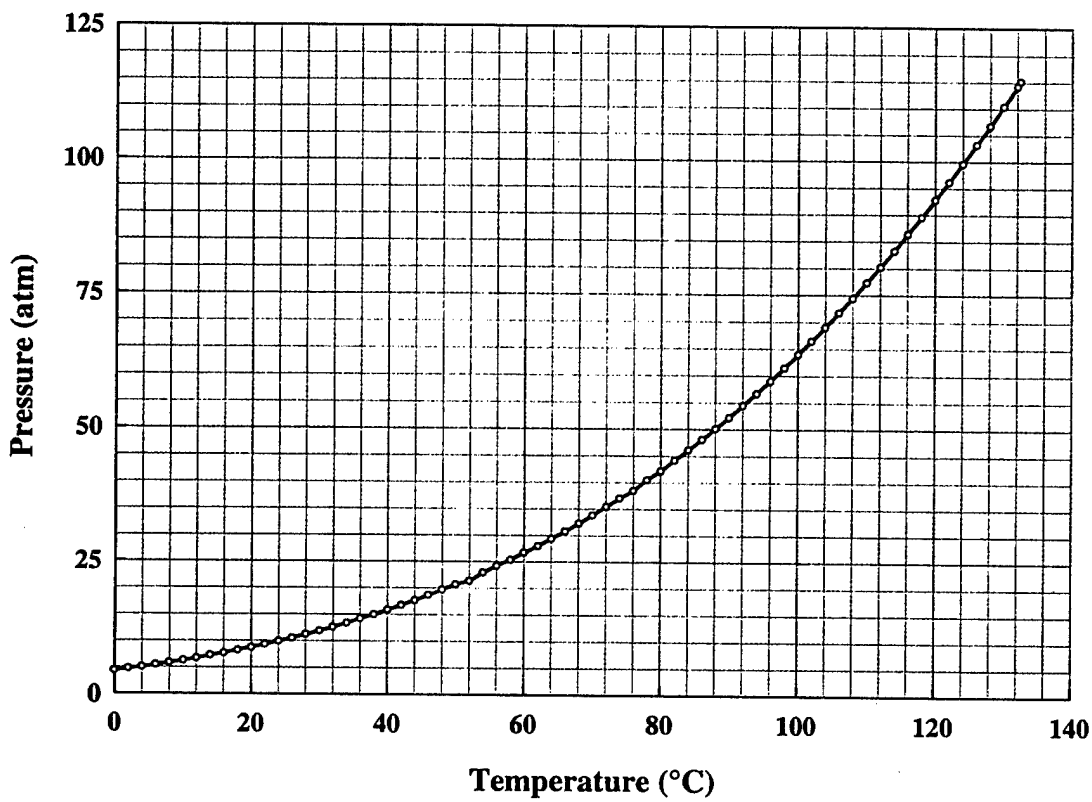

Figure 18. Ammonia vapor pressure curve.[1]

4. Adsorbents

The zeolite used to remove residual ammonia from the reactor effluent stream before it entered the test PEM fuel cell was a type 3A in the form of 16×40 molecular sieve beads from the PQ Corporation. This type A zeolite in the potassium form consists of magnesium aluminum silicate. In addition to the type 3A zeolite, a type 13X in the form of 16×40 molecular sieve beads from the PQ Corporation and an activated carbon from Aldrich were tested to gather ammonia adsorption isotherm data. Table 7 summarizes the three adsorbents analyzed for ammonia adsorption isotherms.

Table 7. Candidate Materials for Ammonia Adsorption

Type	Description	Supplier
3A	Zeolite 16×40	PQ Corporation
13X	Zeolite 16×40	PQ Corporation
Carbon	Activated, 20-40 mesh	Aldrich

5. Reactor Materials

The primary materials used in the construction of the hydrogen-generating catalytic reactor were alumina, aluminum metal, Fiberfrax ceramic cloth, and aerogel insulation. The inner tube for the hydrogen-generating catalytic reactor was obtained from CoorsTek Company. This tube was an extruded alumina tube 6 inches in length and had an outside diameter of 0.25 inches and inside diameter of 0.1875 inches (part # 65658). The outer tube for the reactor was also obtained from CoorsTek Company. This tube, however, had one end closed and was therefore cast alumina; the overall length of the tube was 6.5 inches and had an outside diameter of 0.9375 inches and inside diameter of 0.688 inches (part # 66454). Table 8 contains property data for the alumina tubes. The base for the reactor was machined from a block of standard aluminum and was designed to hold the alumina tubes. The Fiberfrax ceramic cloth was used as a gasketing material to seal the alumina tubes in the reactor base. Finally, aerogel insulation obtained from Aspen Systems was used to insulate the reactor. This aerogel, Pyrogel, is capable of withstanding temperatures up to 3000°C, has a bulk density of only 0.12 g cm^{-3}, and has a thermal conductivity at 38°C of 10 mW m^{-1} K^{-1}.

Table 8. Material Properties for Cast and Extruded Alumina Tubes

Density	3.90 g cm^{-3}
Color	Ivory
Permeability	Gas-Tight
Elastic Modulus at 20°C	350 GPa
Thermal Conductivity at 20°C	30.0 W m^{-1} K^{-1}
Coefficient of Thermal Expansion	8.2×10^{-6} $°C^{-1}$
Specific Heat at 100°C	880 J kg^{-1} K^{-1}

B. Equipment and Procedures

1. Catalyst Preparation

The foam monolithic catalysts and sphere catalysts were prepared in the same manner described by Huff *et. al*[13] in which a metal salt solution is used to wet the catalyst support. The wetted supports were then allowed to dry and next calcined in air at 600 °C for four hours. All supported catalysts were loaded with approximately 10 wt% metal. Figure 19 shows an unloaded foam monolith (white), a loaded foam monolith (green), and the metal solution used to prepare a nickel supported catalyst.

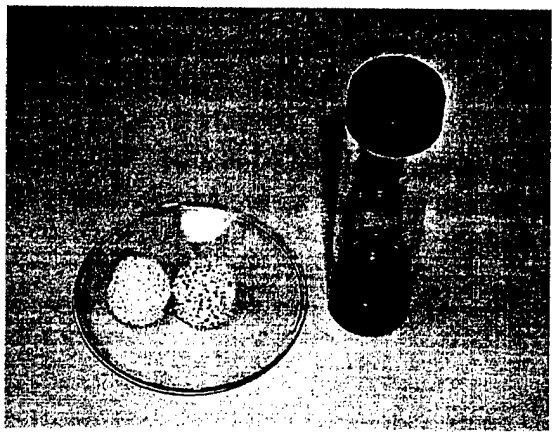

Figure 19. Nickel nitrate solution with foam monoliths.

2. Flow Control

Gas flows (ammonia and air) to the reaction system were controlled with Brooks mass flow controllers. Each gas flow was controlled independently with the gases being introduced to a mixing point so a single reactor feed stream could be generated with virtually any composition. The total feed gas flow rate studied was 2 slpm with varying ammonia:oxygen ratios.

3. Reactor Construction

The base for the hydrogen-generating catalytic reactor was machined from a block of standard aluminum and is designed to hold the alumina tubes with Fiberfrax gaskets. The reactor base had four threaded ports for inlet and outlet gas connections. The outlet port was a 1/4" NPT female port where a 1/4" compression fitting allowed for the connection of the effluent to 1/4" tubing to feed either a bed of adsorbent followed by the PEM fuel cell or a gas chromatograph. The other three ports were 1/8" NPT female ports where 1/8" compression fittings allowed for the connection of feed gases to the reactor. The total weight of the machined aluminum base was 143 grams whereas its overall volume was 63 cm^3. The total mass of the fittings was 85 grams. Refer to Figures 20, 21, 22, and 23 for information pertaining to the reactor base.

Next, the alumina tubes were inserted into the reactor base and gasketed with Fiberfrax. The tubes fit tightly into the base and did not need to be supported. The inner tube weighed 8.2 grams and was loaded with catalyst at the end furthest from the reactor base. The outer tube weighed 71.6 grams and was inserted into the reactor base over the inner tube. The tubes were arranged on the reactor base such that a two-pass coaxial reactor geometry was achieved. Finally, a layer of aerogel insulation was fitted over the outer alumina tube. The final weight and volume of the reactor with compression fittings, loaded with catalyst, and fully insulated was approximately 325 grams and 150 cm^3 respectively.

4. Reactor Startup, Operation, and Shutdown

For a given experiment in which the hydrogen-generating catalytic reactor was tested, the reaction system was started up by first introducing the feed gas at a given ammonia:oxygen ratio to the reactor. Next, a Bunsen burner was started and held below the reactor near the catalyst bed. After a short period of time, ranging from a few seconds to a few minutes, depending on the catalyst and flow rates, the catalyst bed would achieve autothermal operation. Upon autothermal operation, the Bunsen burner was removed and the reactor system was covered with the aerogel insulation. At this point the reactor could be used for experimentation through the analysis of the effluent. Once autothermal operation was attained, the feed gas composition and total flow rate could be varied through changes made to the mass flow controllers. Shutdown of the reaction system was achieved by simply turning off the feed gas supply.

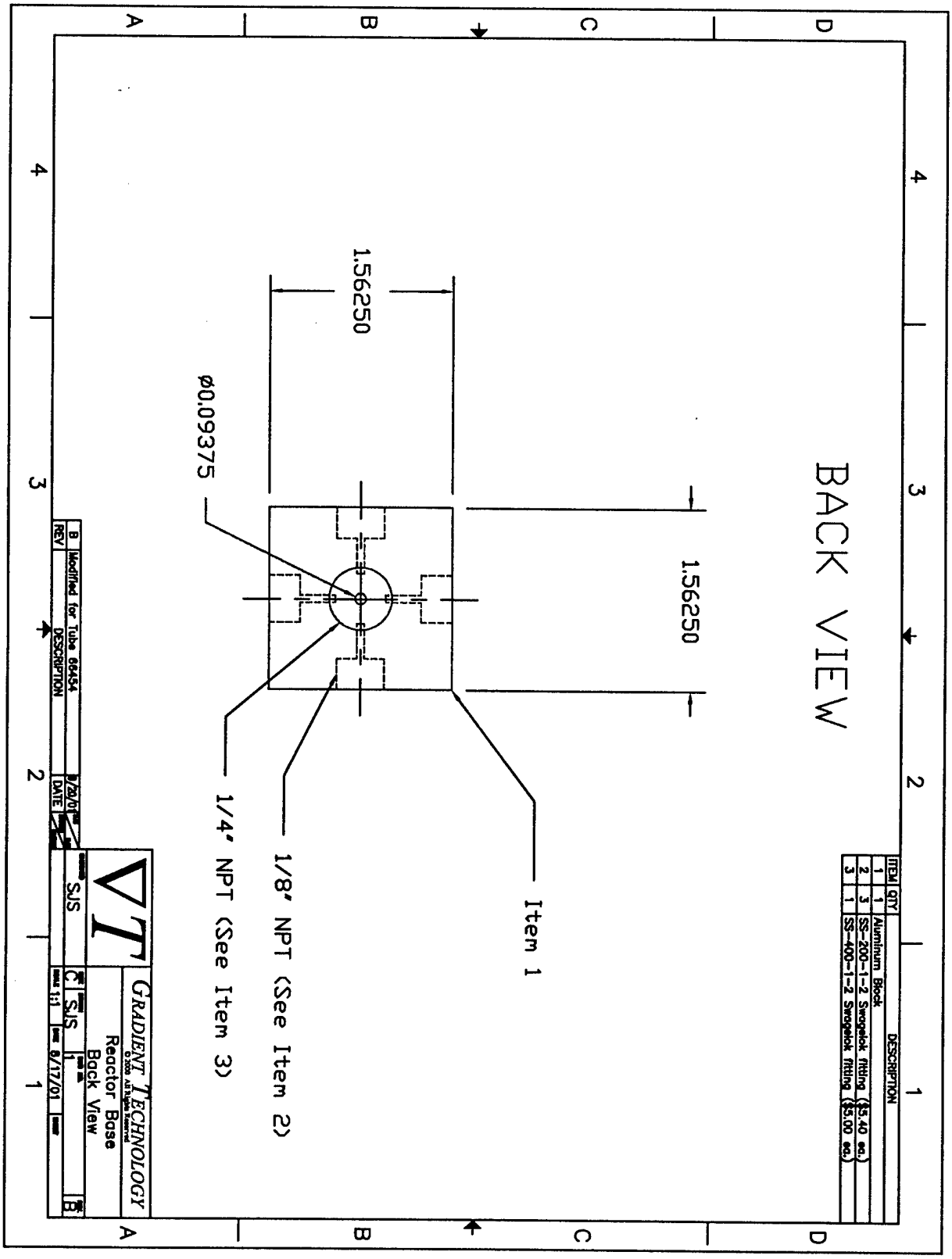

Figure 20. Reactor base back view.

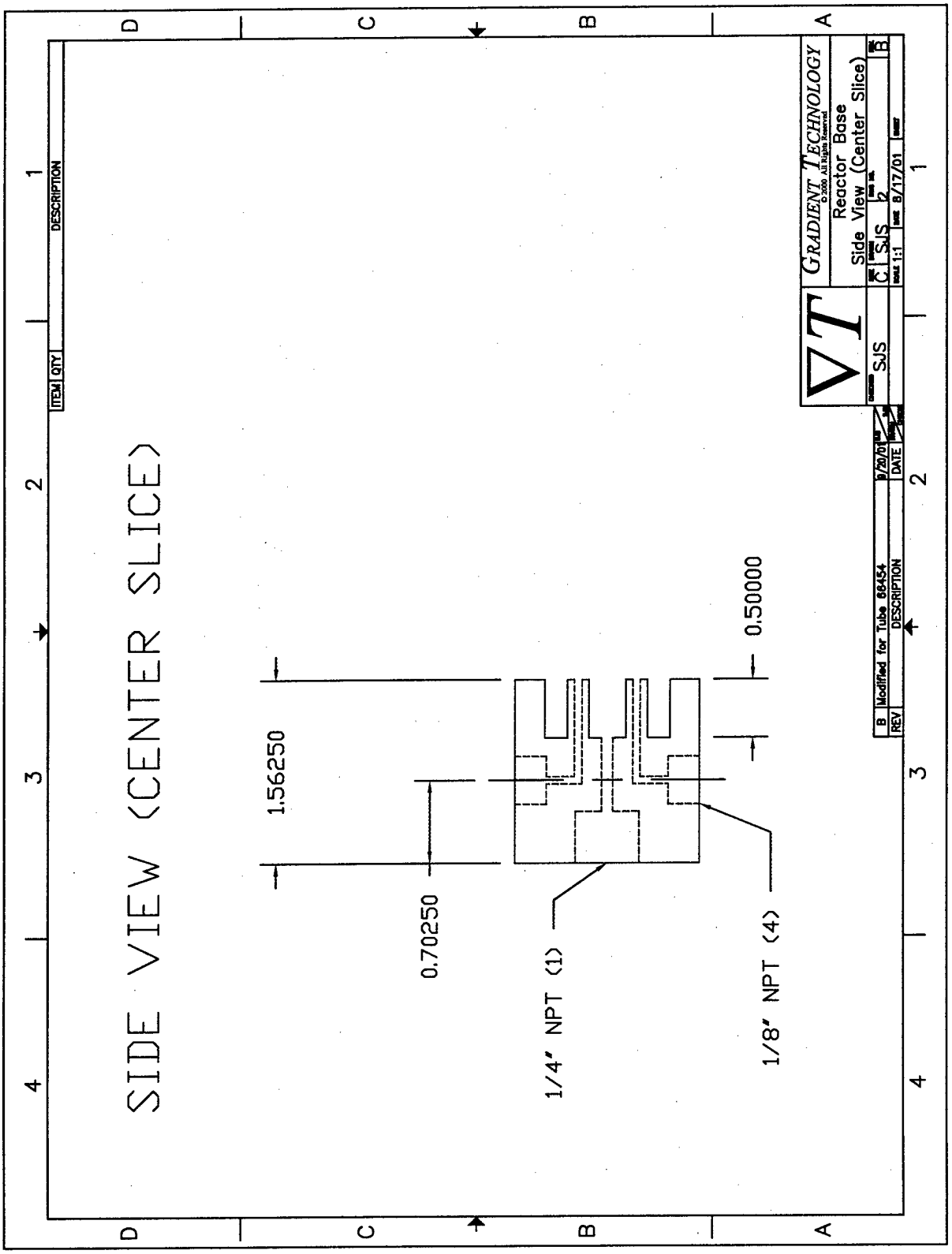

Figure 21. Reactor base side view (center slice).

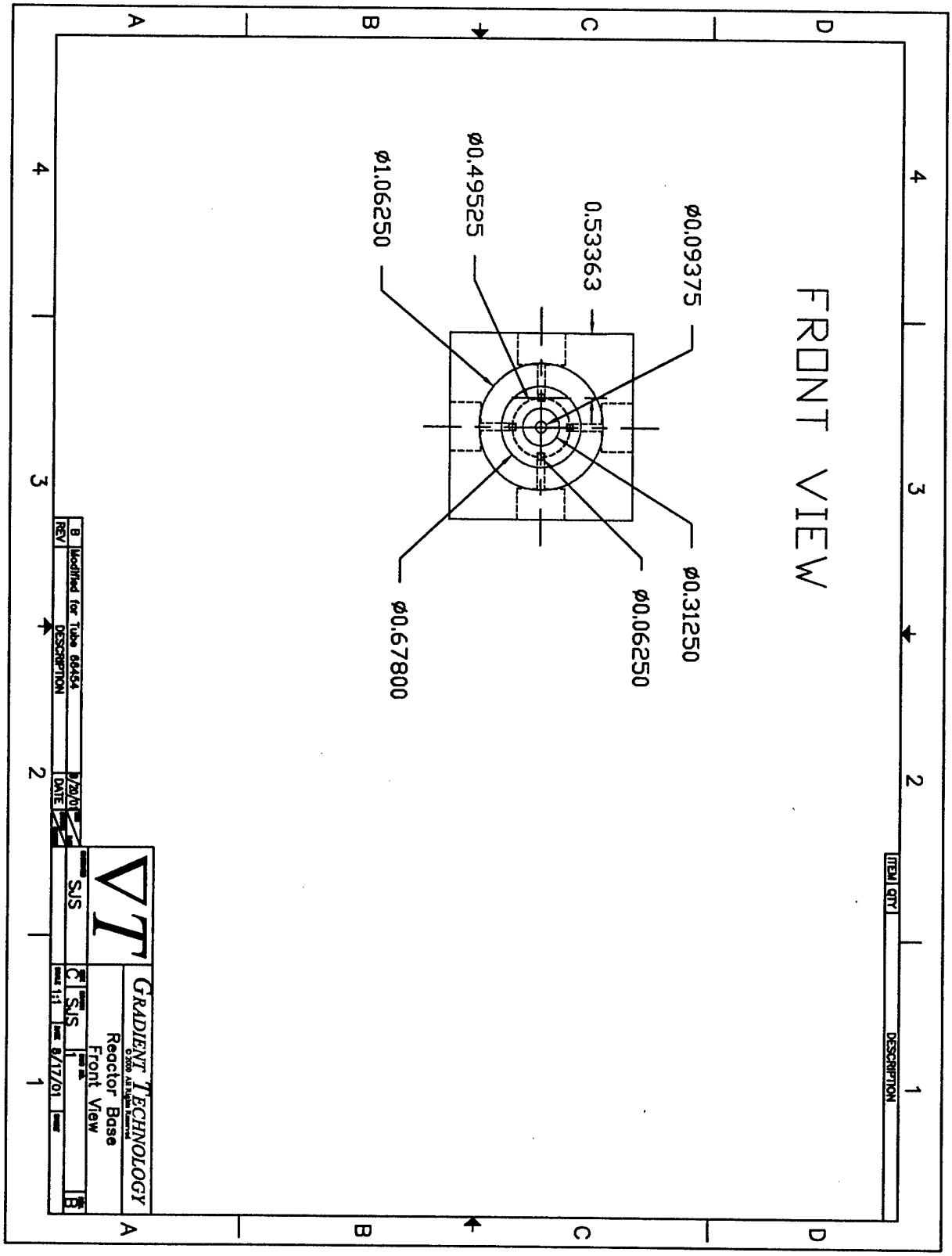

Figure 22. Reactor base front view.

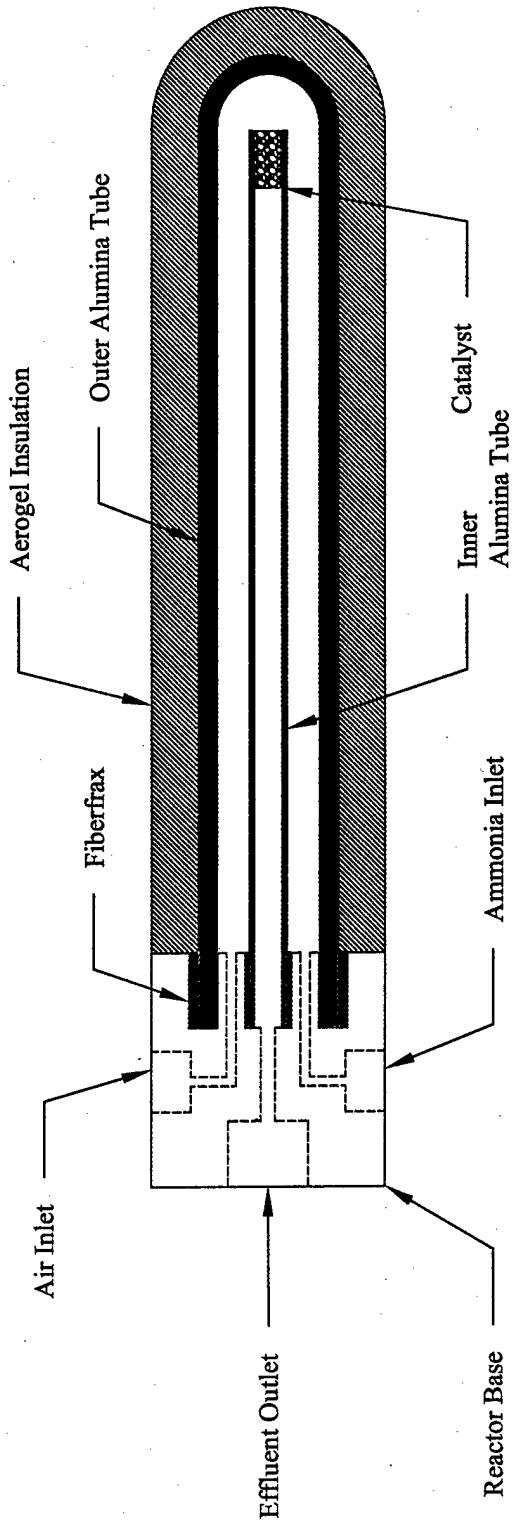

Figure 23. Hydrogen-generating catalytic reactor.

5. Gas Analysis

Effluent from the reaction system was analyzed with a Hewlett-Packard 5890 gas chromatograph fitted with a HayeSep D 30'x1/8" column. The gases analyzed for included hydrogen, oxygen, nitrogen, ammonia, water, and nitrogen oxides. For analytical purposes argon was used instead of nitrogen in the feed gas so that the nitrogen content of the reactor effluent could be analyzed.

6. Micro Air Pumps

Two micro air pumps for providing air to the hydrogen-generating catalytic reactor were tested. These pumps were purchased from Sensidyne. Table 9 contains data pertaining to these micro air pumps and figure 24 contains a picture of the AA Series pump. Note that these pumps were powered through an independent power supply. Connection of an air pump to the reactor base was straightforward; the outlet of the pump was connected with tubing to a small needle valve that was subsequently connected to the air inlet on the reactor base.

7. Fuel Cell and Testing

Upon the completion of the design, fabrication, and testing of the hydrogen-generating catalytic reactor with various catalysts, the reactor was loaded with a nickel sphere bed. Next the reactor outlet was plumbed through a zeolite bed (to ensure no ammonia reached the fuel cell) and on to the PEM fuel cell. Initial testing was done using a single membrane electrode assembly with a platinum anode and a platinum cathode (see figure 25). Subsequent testing was done utilizing a 50 Watt PEM fuel cell from ElectroChem, Inc (see figure 26).

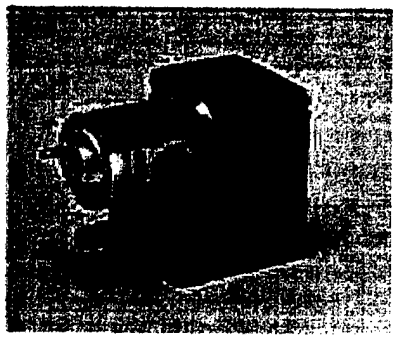

Figure 24. Micro air pump used to deliver air to the hydrogen-generating catalytic reactor.

Table 9. Micro Air Pump Specifications

	AA120INSNF50PC1	AAA120INSNF30PC1
Model	50	30
Minimum Free Flow	2660 cm^3 min^{-1}	815 cm^3 min^{-1}
Minimum Pressure @ Dead Head	6.3 psig	6.3 psig
Maximum Current @ Free Flow	120 mA	30 mA
Rated Voltage	12.0 VDC	12.0 VDC
Motor Construction	Ironless Rotor	Ironless Rotor
Diaphragm Material	Neoprene	Neoprene
Pump Body Material	Ryton	Ryton
Temperature Range	0°C - 50°C	0°C - 50°C
Weight	35 grams	30 grams
Size	23 cm^3	18 cm^3

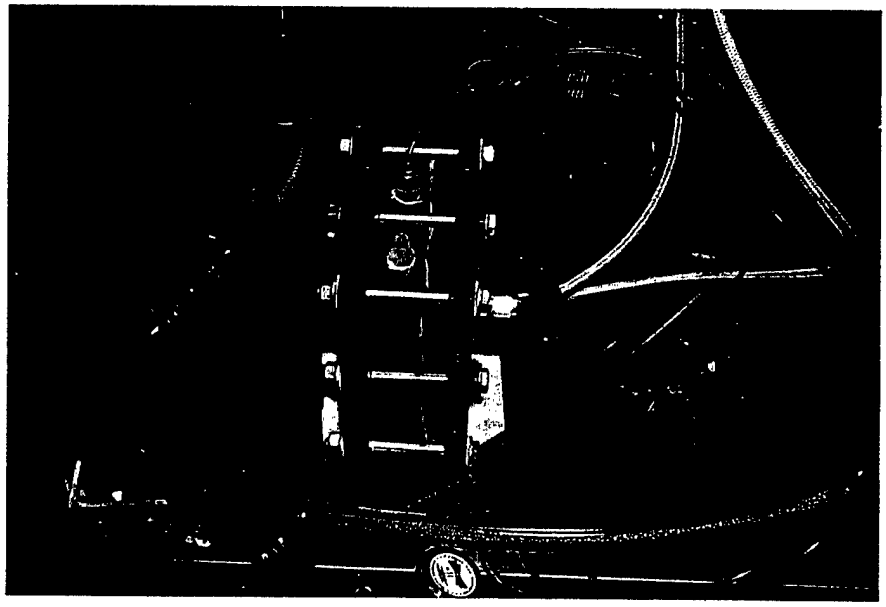

Figure 25. Single cell PEM fuel cell coupled to the hydrogen-generating catalytic reactor.

Figure 26. Experimental 50 Watt PEM fuel cell.

8. Adsorption Isotherms

Ammonia adsorption isotherms were collected at two temperatures (25°C and 100 °C) for the adsorbents listed in table 7. This data was collected using a Quantachrome Autosorb-1-C Chemisorption-Physisorption Analyzer (see figure 27). To collect an adsorption isotherm, a sample of adsorbent was outgassed and weighed. Finally, ammonia at increasing pressures was added to the sample. The Autosorb automatically increased the pressure and measured equilibrium pressures.

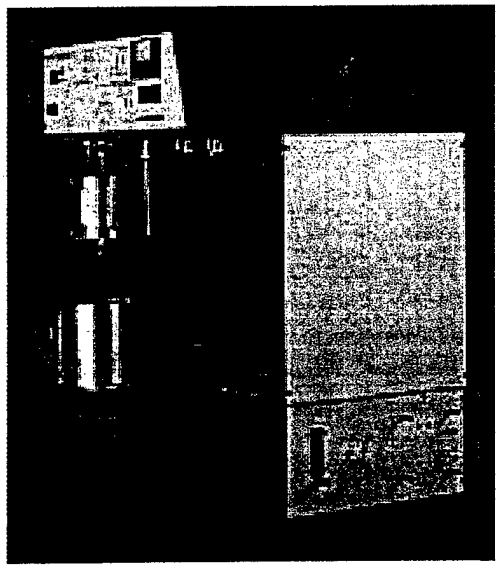

Figure 27. Quantachrome Autosorb 1-C Chemisorption-Physisorption Analyzer used to collect ammonia adsorption isotherms.

9. Ammonia Storage Canister

An ammonia storage canister was fabricated from type 3003 aluminum and tested with ammonia. Type 3003 aluminum has excellent resistance to chemical attack and is a frequent choice in the manufacture of chemical equipment. In addition, the weldability of type 3003 aluminum is excellent. The storage canister consisted of a piece of 3 inch outside diameter aluminum tube with end caps welded on. One cap had two aluminum 1/4" NPT couplings welded on to it for a pressure gauge/vent and a fill valve. The internal volume of the canister was 363 cm^3 and its empty weight was 278 grams. The canister was hydrostatically tested to 150 psig and subsequently filled with ammonia; a standard cylinder of ammonia was attached to the canister that was chilled in an alcohol/dry ice bath.

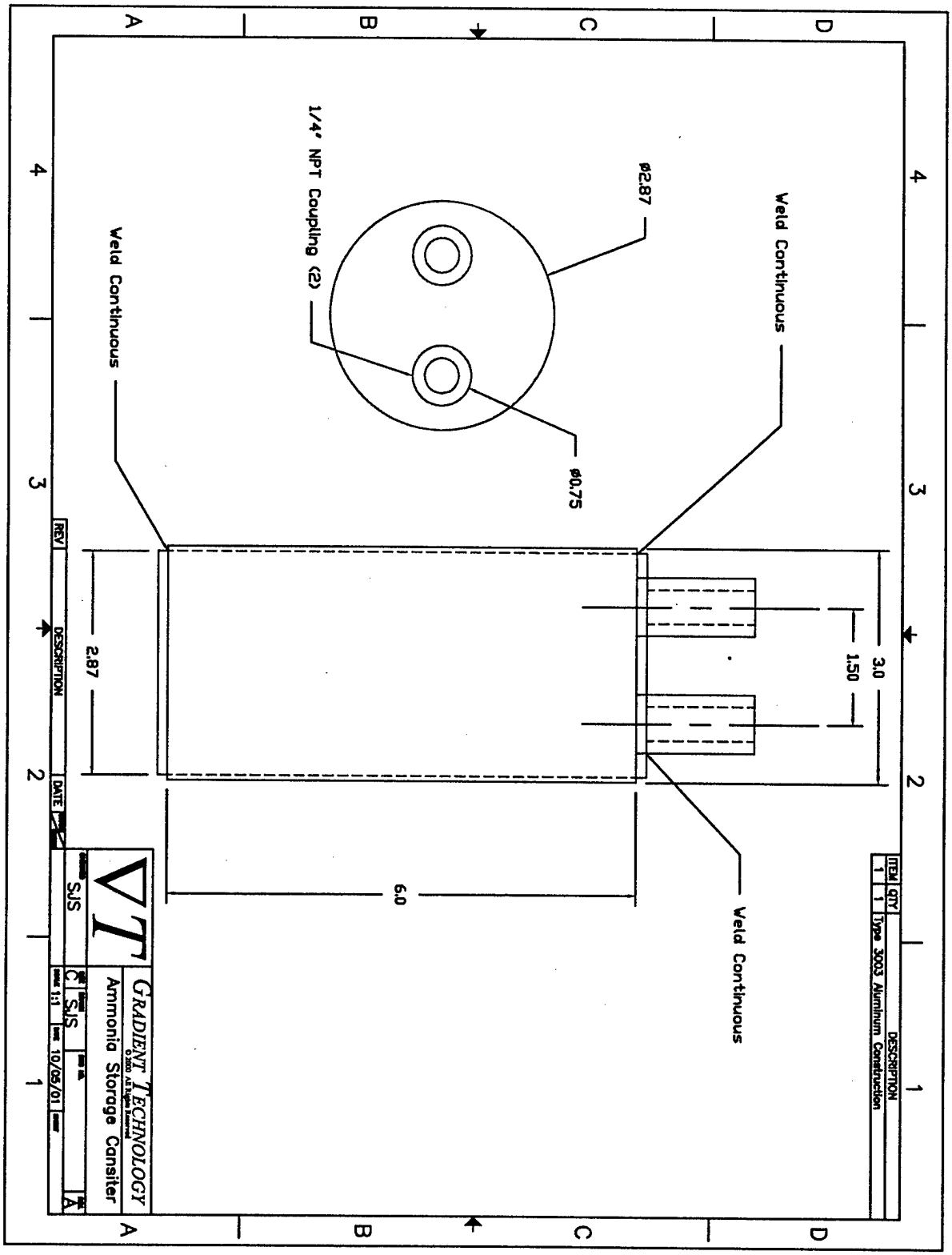

Figure 28. Ammonia storage canister.

IV. RESULTS AND DISCUSSION

The experimental results of this research are summarized and discussed in this section of the report. The performance of the hydrogen-generating catalytic reactor is discussed in terms of ammonia conversion and selectivity to hydrogen as defined in tables 3 and 4. In addition the coupling of the reactor to a PEM fuel cell is discussed. Finally, ammonia adsorption isotherm data is presented along with some thoughts on ammonia storage.

A. Reactor Performance

Initially, a two-pass coaxial quartz reactor was used to test various catalysts. After screening additional catalysts, the reactor consisting of alumina tubes and a reactor base as described previously was constructed and tested.

1. Ruthenium

Two supported ruthenium catalysts were prepared and tested at 2 slpm in the two-pass coaxial quartz reactor with varying ammonia:oxygen ratios. For these tests air was supplied from a cylinder. One support consisted of the 80 pores per inch monolith, whereas the other support consisted of 1 mm alumina spheres. Both catalysts performed similarly as shown in figures 29 and 30.

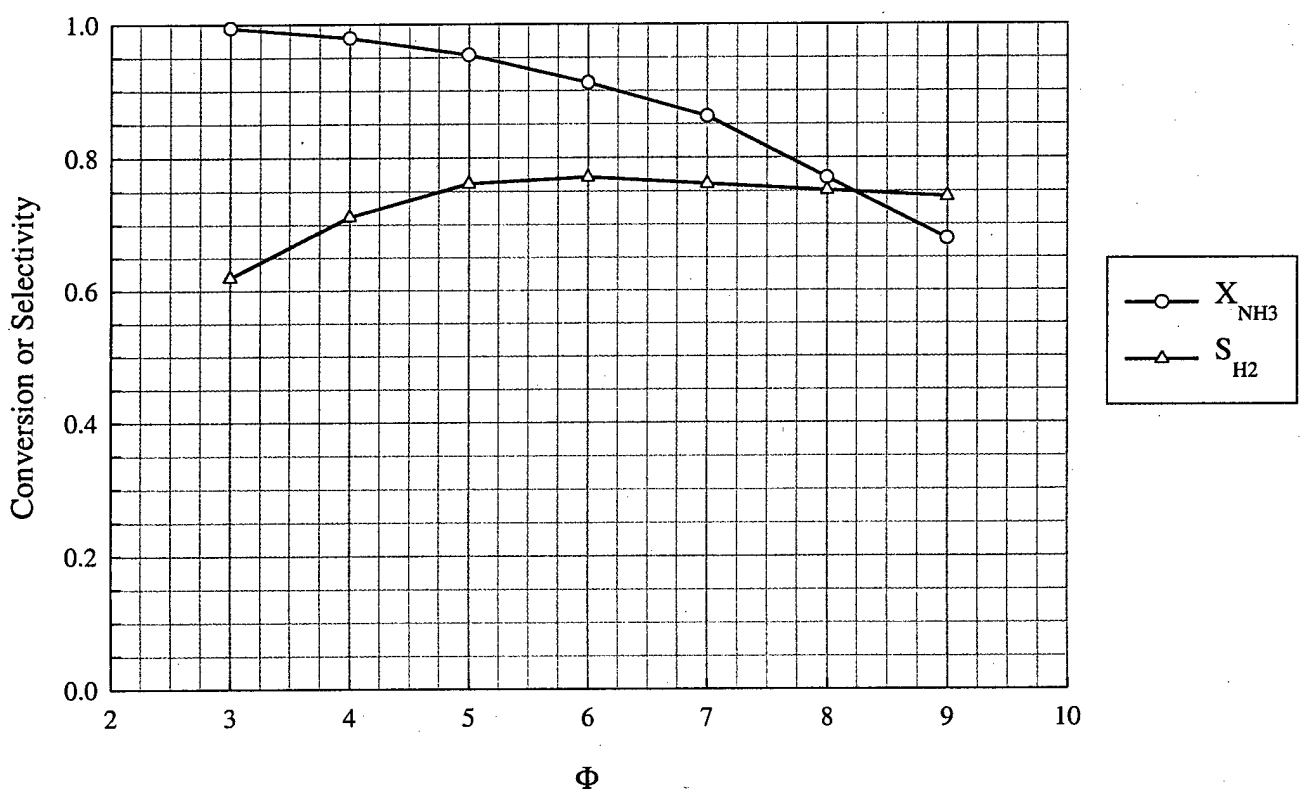

Figure 29. Ruthenium foam monolith catalyst performance in the two-pass coaxial quartz reactor.

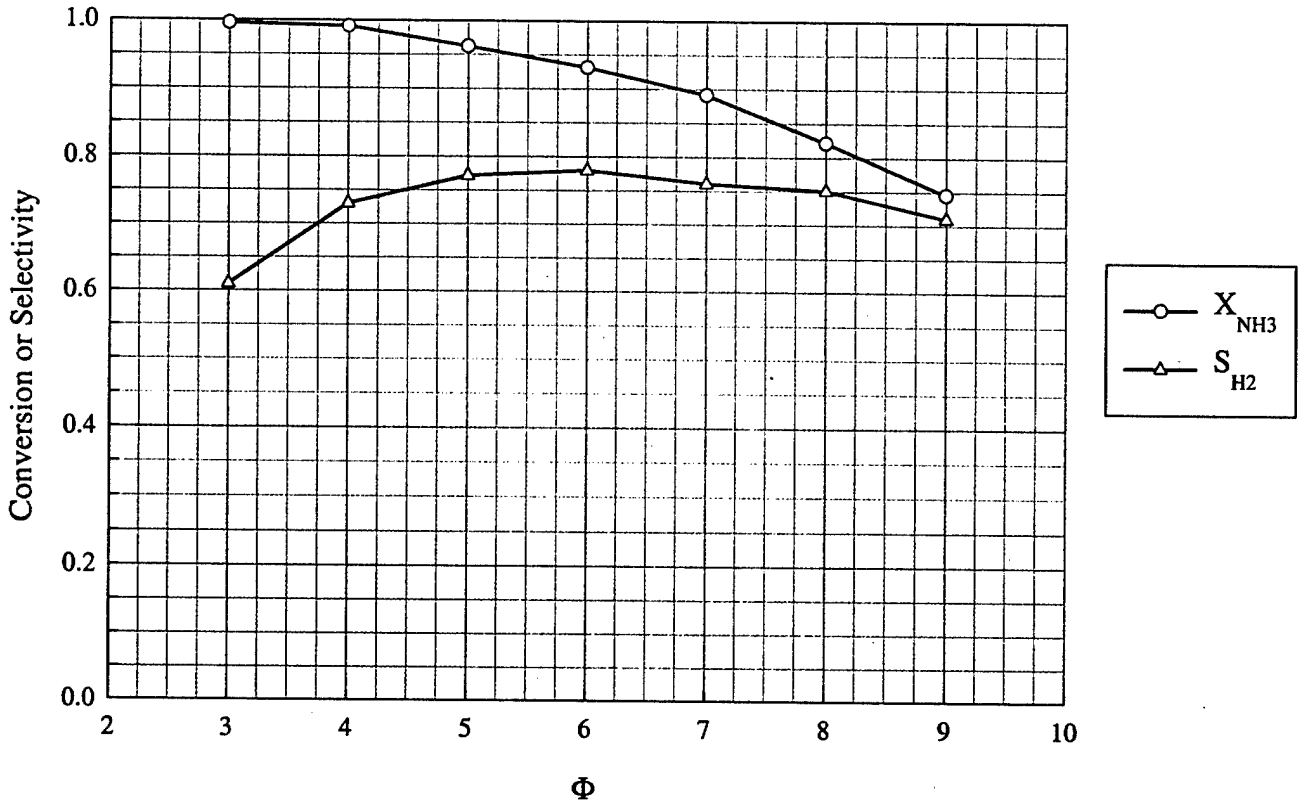

Figure 30. Ruthenium sphere bed catalyst performance in the two-pass coaxial quartz reactor.

From this data it can be easily seen that these two catalysts performed in a similar fashion. The sphere bed, however, yielded a slightly higher selectivity at lower ammonia:oxygen ratios.

2. Nickel

Two supported nickel catalysts were prepared and tested at 2 slpm in the two-pass coaxial quartz reactor with varying ammonia:oxygen ratios. For these tests air was supplied from a cylinder. One support consisted of the 80 pore per inch monolith, whereas the other support consisted of 1 mm alumina spheres. The results of the nickel catalyst experiments are shown in figures 31 and 32.

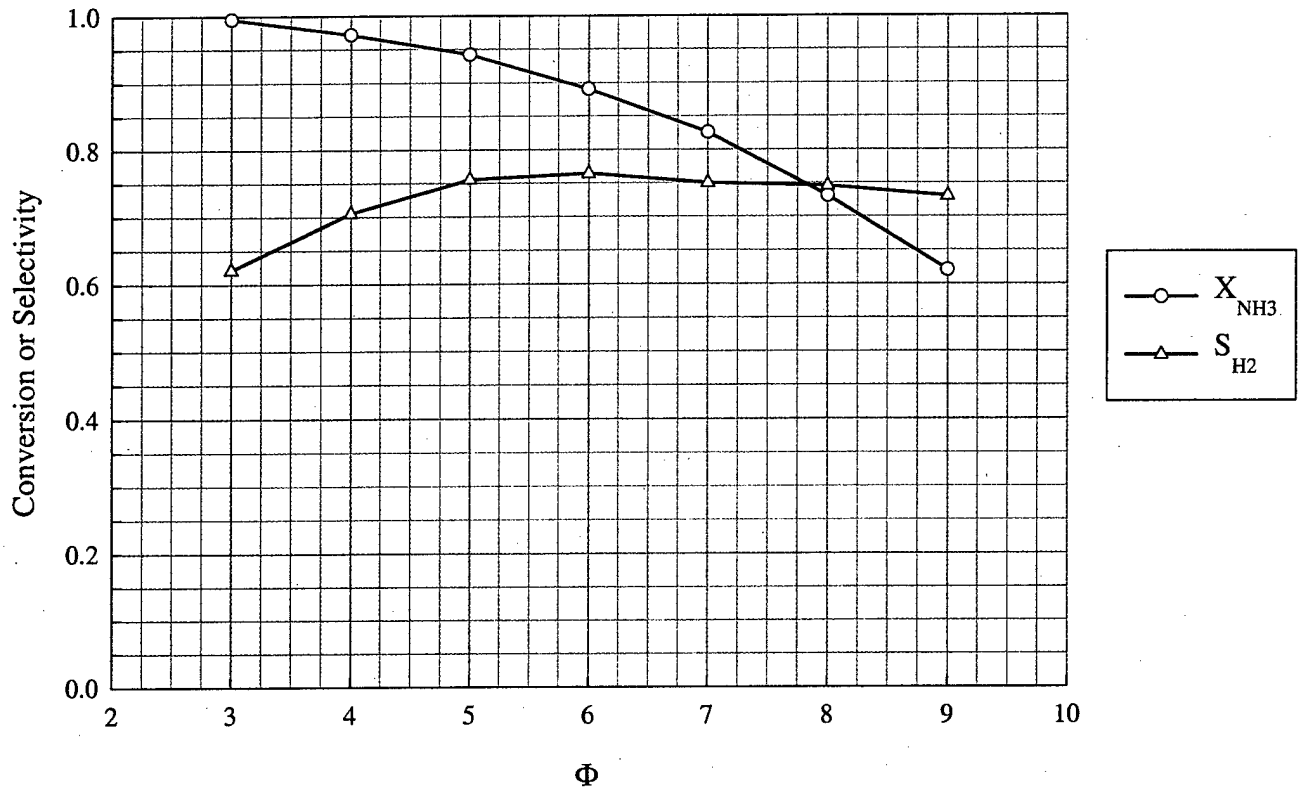

Figure 31. Nickel foam monolith catalyst performance in the two-pass coaxial quartz reactor.

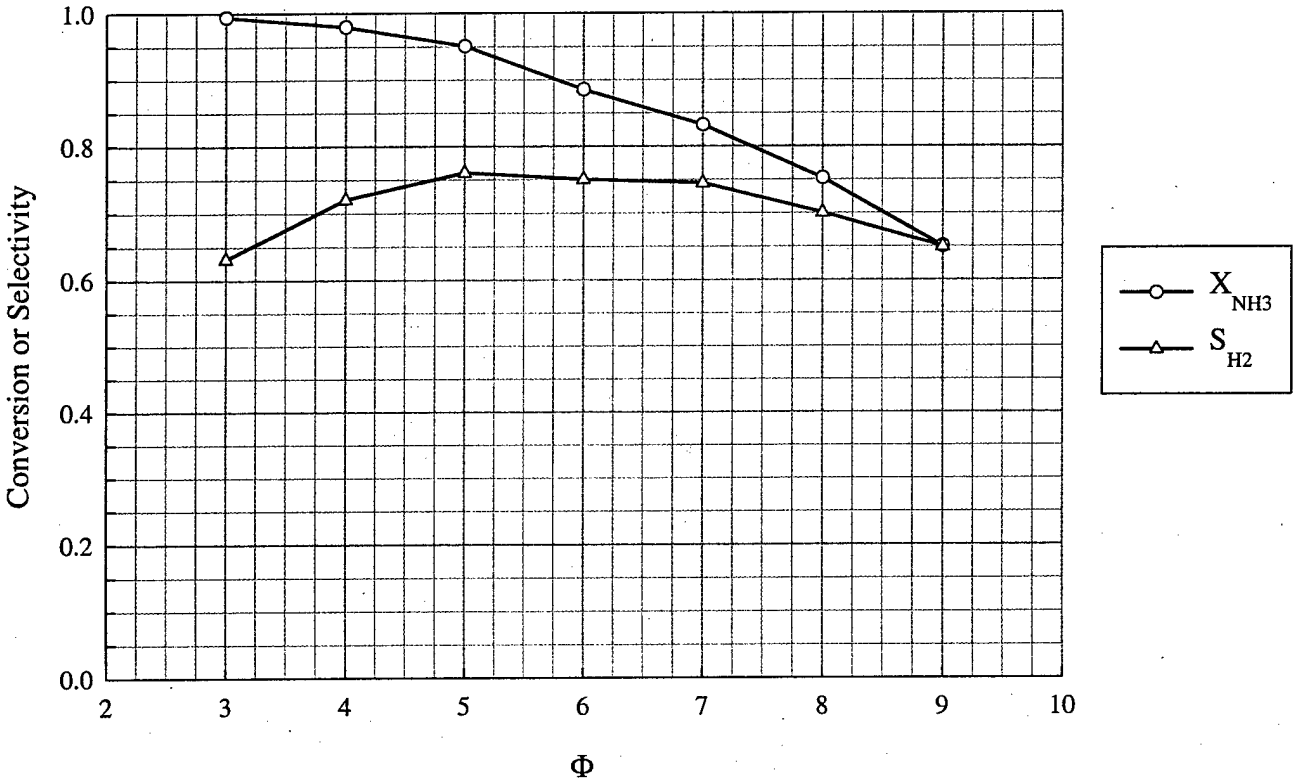

Figure 32. Nickel sphere bed catalyst performance in the two-pass coaxial quartz reactor.

From this data for the nickel catalysts it appears that the monolithic catalyst performed slightly better than the sphere bed at all ammonia:oxygen ratios *i.e.* the monolithic catalyst operated at slightly higher conversions of ammonia and selectivities to hydrogen.

3. Nickel Gauze

Lastly, a woven nickel gauze catalyst was tested. In order to test the gauze catalyst (pure nickel), disks of the gauze were sandwiched in between two inactive foam monoliths. As in the other experiments, the total flow rate of feed gases to the reactor was 2 slpm. The results for the gauze catalyst are shown in figure 33 and are very similar to the supported nickel catalysts.

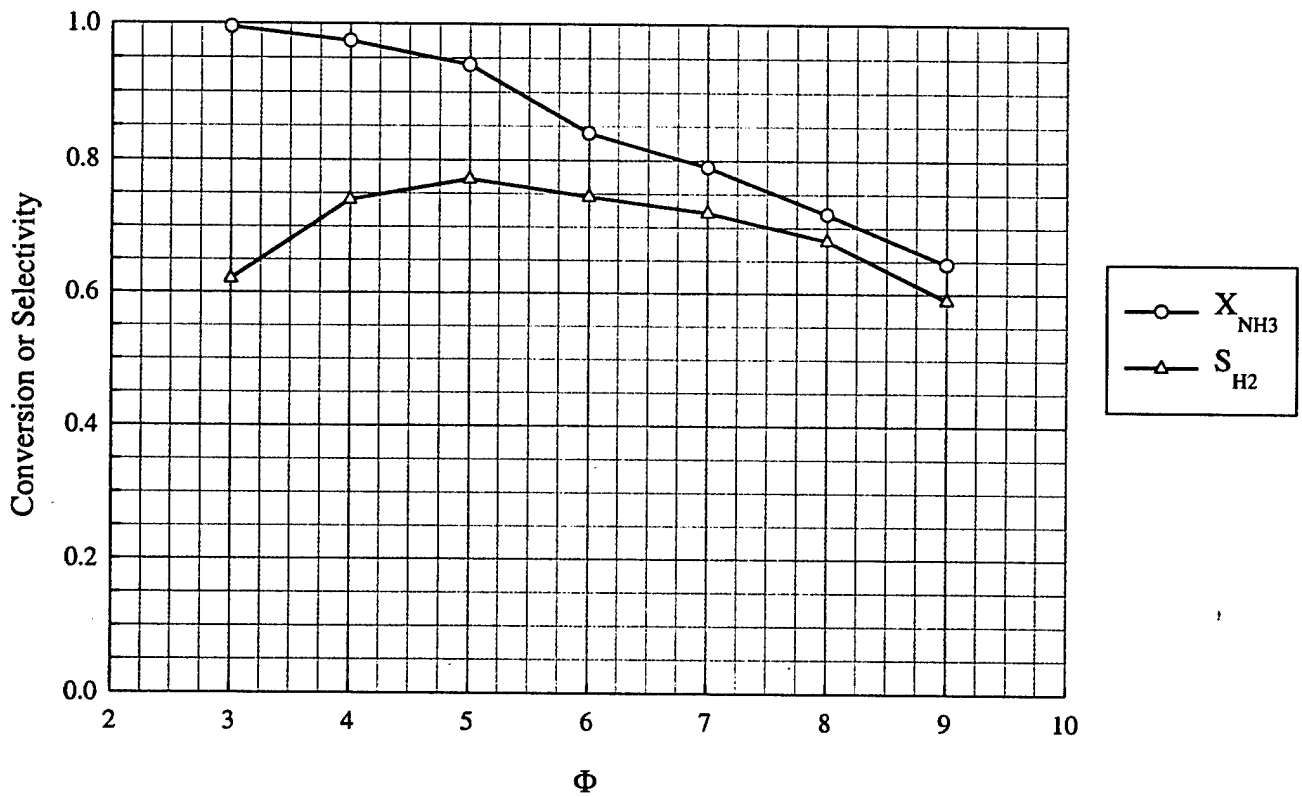

Figure 33. Nickel woven gauze catalyst performance in the two-pass coaxial quartz reactor.

4. Alumina Tube Reactor

Upon completion of the design and fabrication of the alumina tube reactor previously described, a nickel sphere bed was packed into the tip of the inner alumina tube. This reactor was operated in a similar fashion as the quartz reactor in that ammonia and air were supplied from cylinders and a Bunsen burner had to be used to start the reactor. After the reactor was started insulation was placed around it to minimize heat losses. Once again, the ammonia:oxygen ratio was varied while keeping the total flow rate at 2 slpm. The data for these experiments is shown in figure 34.

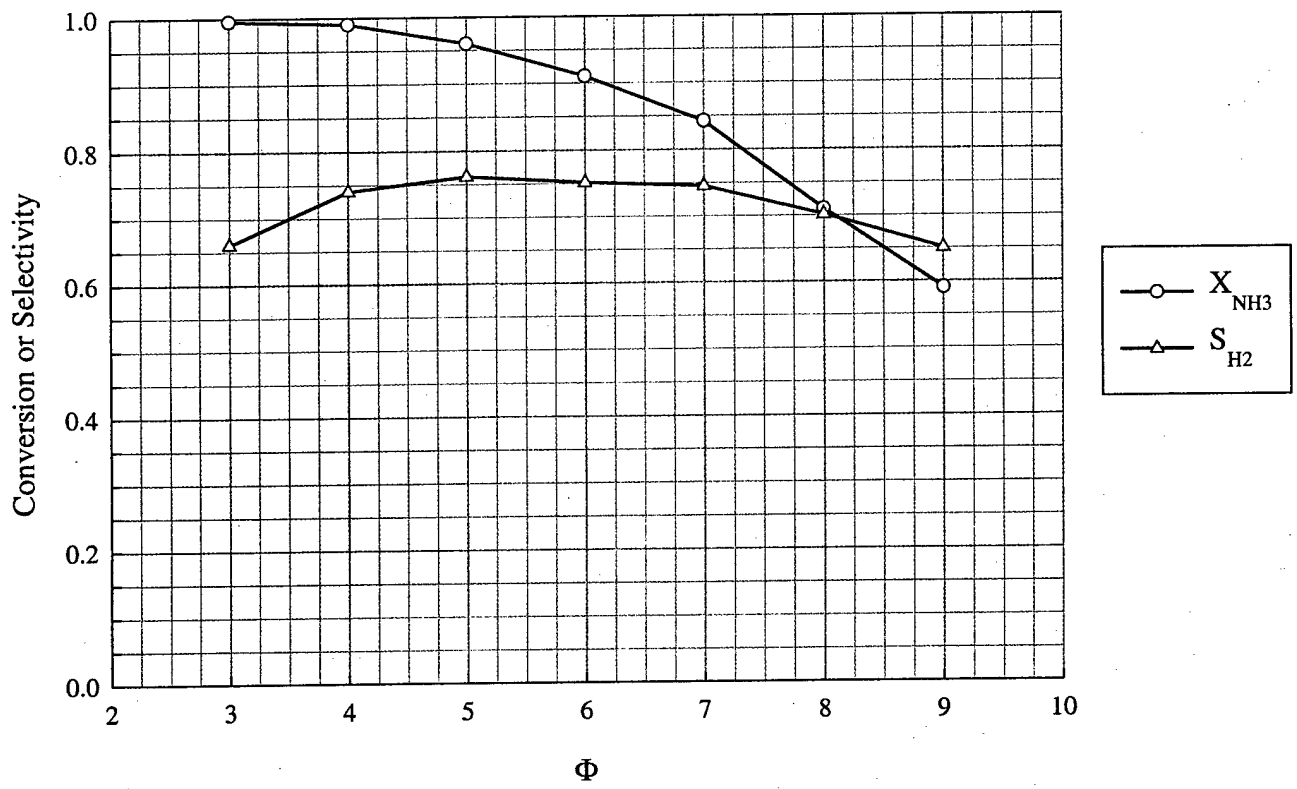

Figure 34. Nickel sphere bed catalyst performance in the alumina tube reactor.

Ideally, one would like to operate the reactor at higher ammonia:oxygen ratios so less ammonia is oxidized completely to water and nitrogen. Thus, numerous attempts were made to enhance the performance of the reactor through various insulating techniques which included the placement of a quartz vacuum jacket on the outside of the reactor. As it turns out, the relatively simple idea of putting a vacuum jacket on the outside of the reactor turned out to be very difficult. As a result of difficulties in the fabrication and attachment of the jacket to the reactor, simple aerogel insulation was chosen and the reactor was operated at an ammonia:oxygen ratio of four.

The next piece of the hydrogen-generating catalytic reactor system to be tested before operation

with a fuel cell was the micro air pumps. These pumps were initially tested independent of the reaction system to verify they would deliver the necessary air to the reactor. Data for the micro air pump performance is shown in figures 35 and 36.

The AA micro air pump needs to supply about 1.1 slpm of air to the reactor. This pump was attached to the alumina tube reactor and tested with the simultaneous feed of ammonia. Flow of air was achieved through the reactor with a needle valve, however, steady flows were somewhat difficult to achieve. Since a check valve in the air line to the reactor would provide too much back pressure for the micro air pump, the system was operated without one; thus it was important to turn the air flow on before the ammonia to prevent ammonia from flowing back to the air pump. Nonetheless, additional time needs to be spent on supplying air to the reactor with these air pumps.

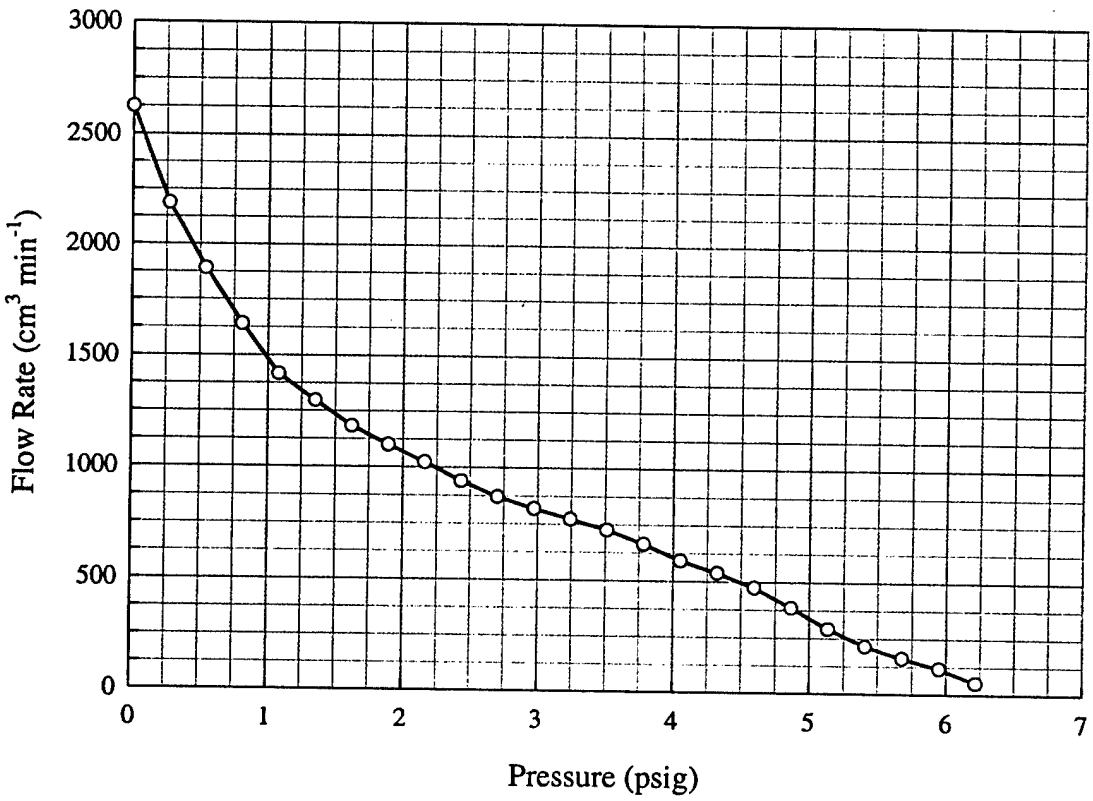

Figure 35. AA Micro air pump performance data.

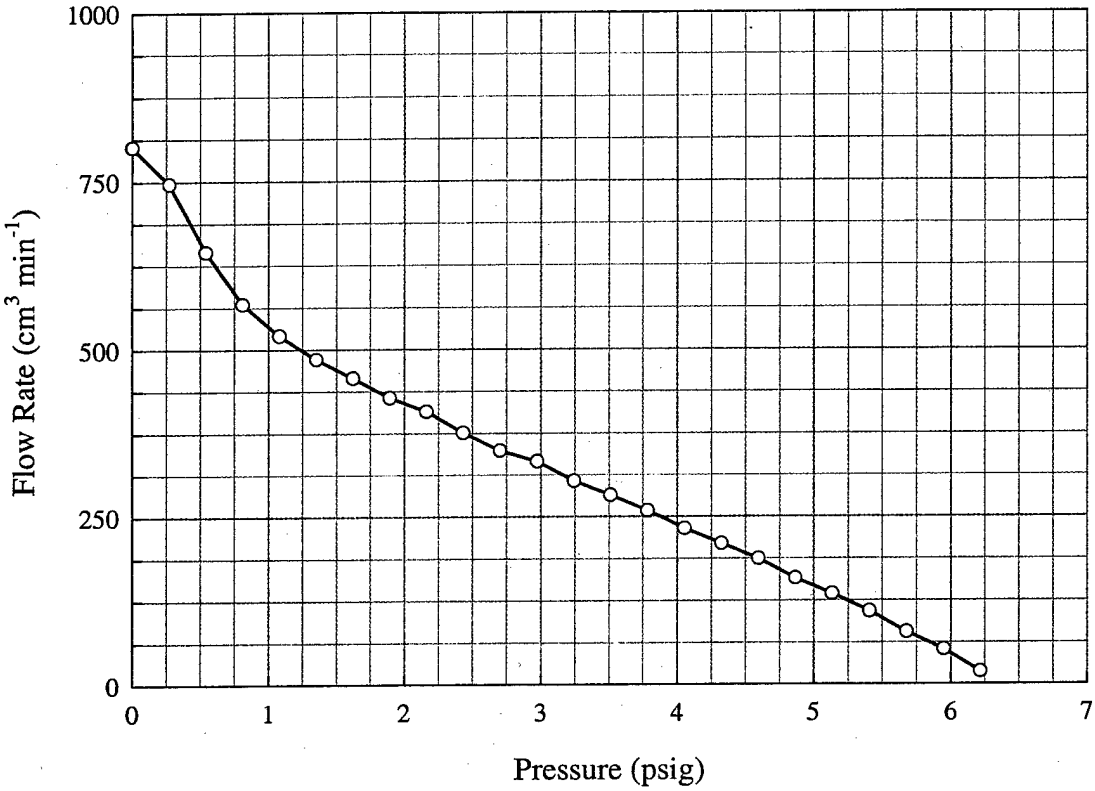

Figure 36. AAA Micro air pump performance data.

B. Fuel Cell Testing

The alumina tube reactor was initially attached to a single membrane electrode assembly. The reactor was operated at an ammonia:oxygen ratio of 4 and a total flow rate of 2 slpm. Also, the reactor effluent was passed through a zeolite bed to prevent any ammonia from reaching the MEA. For this and subsequent tests air was supplied from a cylinder. During operation of the reactor, an open circuit voltage of 0.820 Volts was achieved.

Next, the reactor system was coupled to a 50 Watt PEM fuel cell stack with the goal of powering it to 30 Watts. This fuel cell had 7 cells each with an area of 50 cm^2 yielding a total area of 350 cm^2. This fuel cell also did not require an external humidification. Figure 37 contains power, current density, and voltage data for the 50 Watt PEM fuel cell stack.

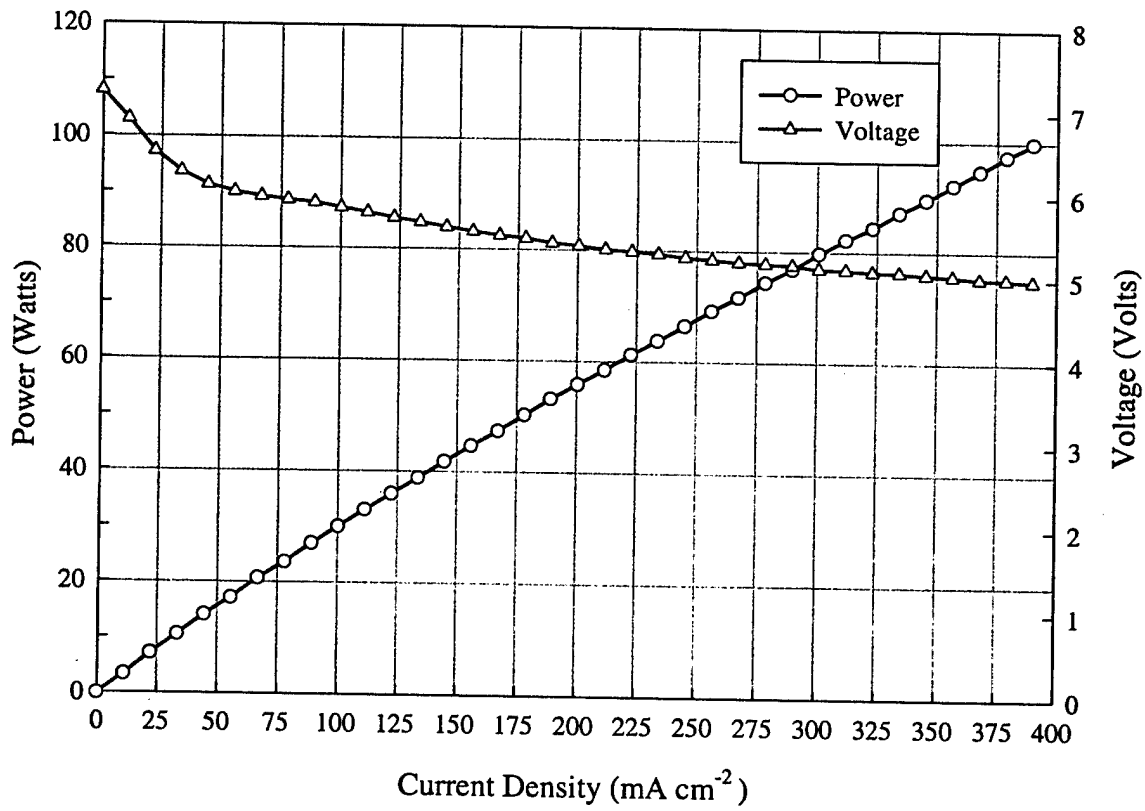

Figure 37. Power output of the PEM fuel cell stack.

Testing of the fuel cell stack with the alumina tube reactor involved placing a load on the fuel cell and measuring the stack voltage and current output. Based on figure 37, a 30 Watt output with the fuel cell consisting of 7 cells will require 1.87×10^{-4} moles hydrogen sec^{-1}. Table 10 summarizes the reactor operating conditions and performance when attached to the fuel cell.

Table 10. Reactor Performance for Fuel Cell Test

Ammonia:Oxygen Ratio	4
Total Feed Rate	2 slpm
Ammonia Feed Rate	0.91 slpm
Air Feed Rate	1.09 slpm
Catalyst	Nickel supported on alumina spheres
Gas Hourly Space Velocity	6.0×10^{5} hr^{-1}
Ammonia Conversion	~99%
Selectivity to Hydrogen	~72%
Hydrogen Production Rate	6.74×10^{-4} moles hydrogen sec^{-1}

During the test of the fuel cell, a current of 6.4 amps at 5.7 volts was measured. Based on this data and the fuel cell information in figure 37, hydrogen was being consumed in the fuel cell at a rate of 6.74×10^{-4} moles hydrogen sec^{-1}. Overall, the reactor successfully powered the fuel cell.

C. Ammonia Adsorption

A total of six adsorption isotherms were collected for three materials. The temperatures investigated were 25°C and 100°C. The following six figures plot the isotherm data. Based on the data presented in the isotherm plots, all three materials adsorb ammonia in a similar fashion. At 25°C the 13X zeolite appears to have the most capacity at atmospheric pressure (approximately 143 $cm^3 g^{-1}$). At 100°C all three adsorbents performed about the same (approximately 113 $cm^3 g^{-1}$). If the 13X zeolite were chosen as an adsorbent for ammonia, at 25°C one would require approximately 9 grams of adsorbent to capture one gram of ammonia.

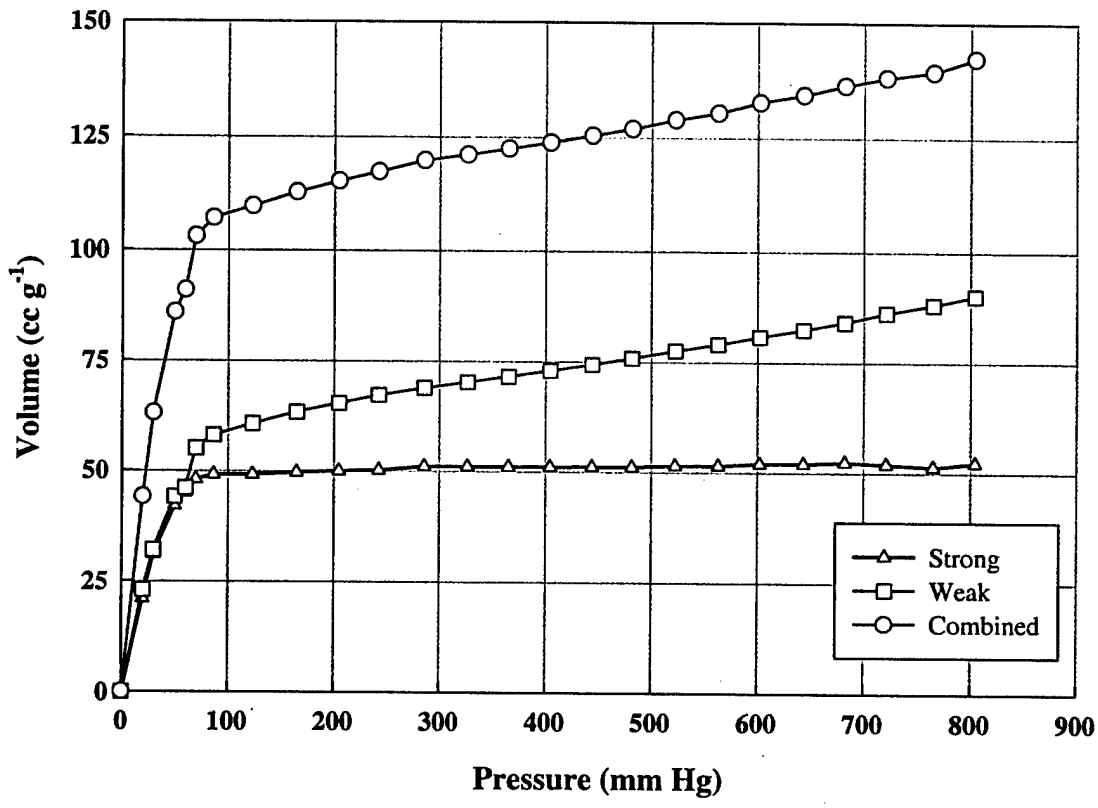

Figure 38. Ammonia adsorption isotherm at 25°C on type 3A zeolite.

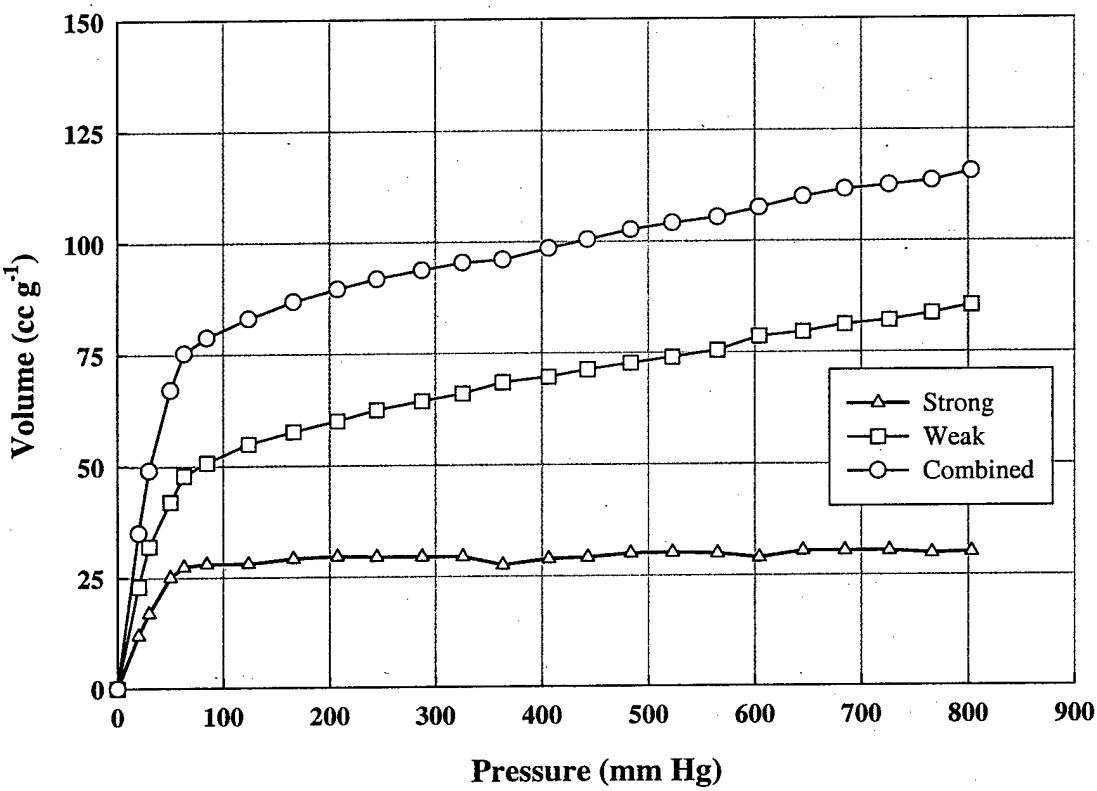

Figure 39. Ammonia adsorption isotherm at 100°C on type 3A zeolite.

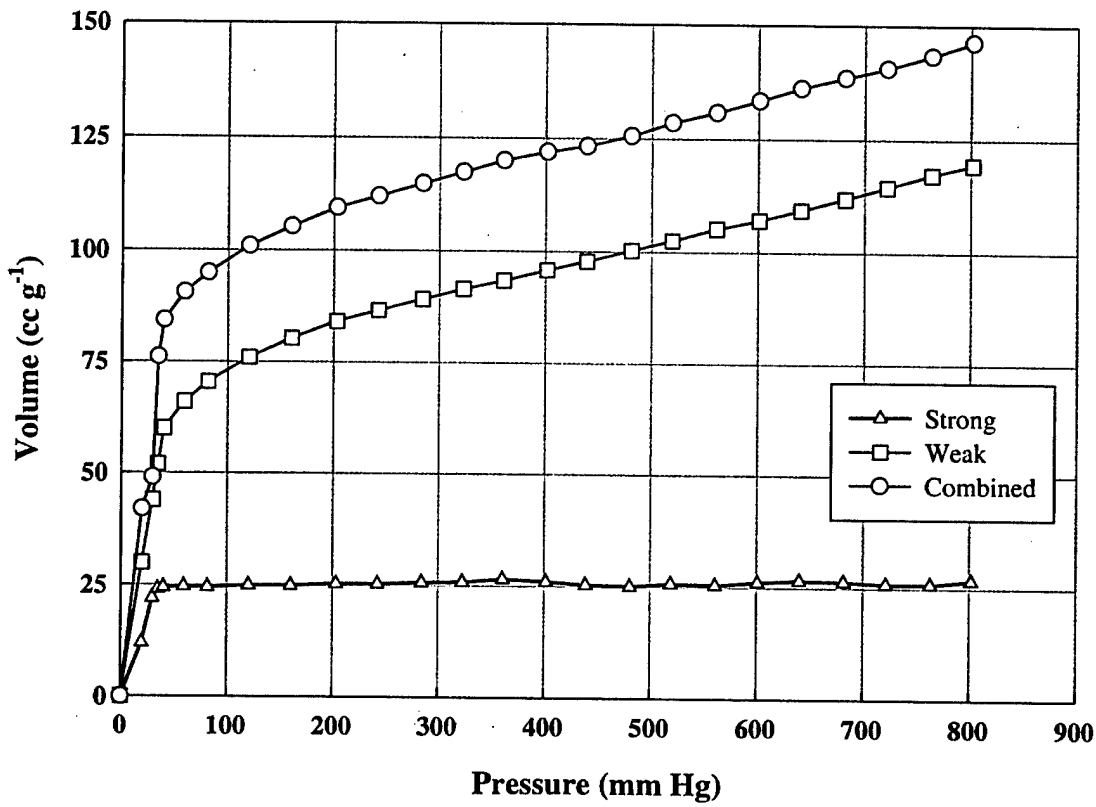

Figure 40. Ammonia adsorption isotherm at 25°C on type 13X zeolite.

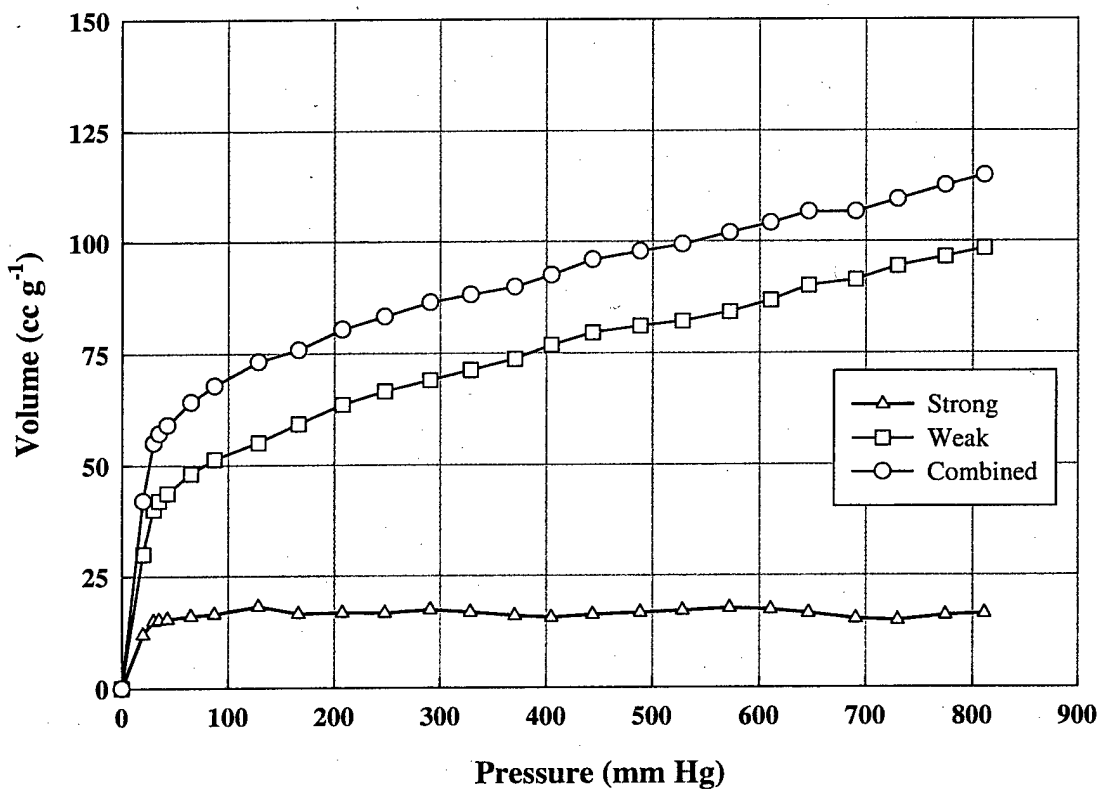

Figure 41. Ammonia adsorption isotherm at 100°C on type 13X zeolite.

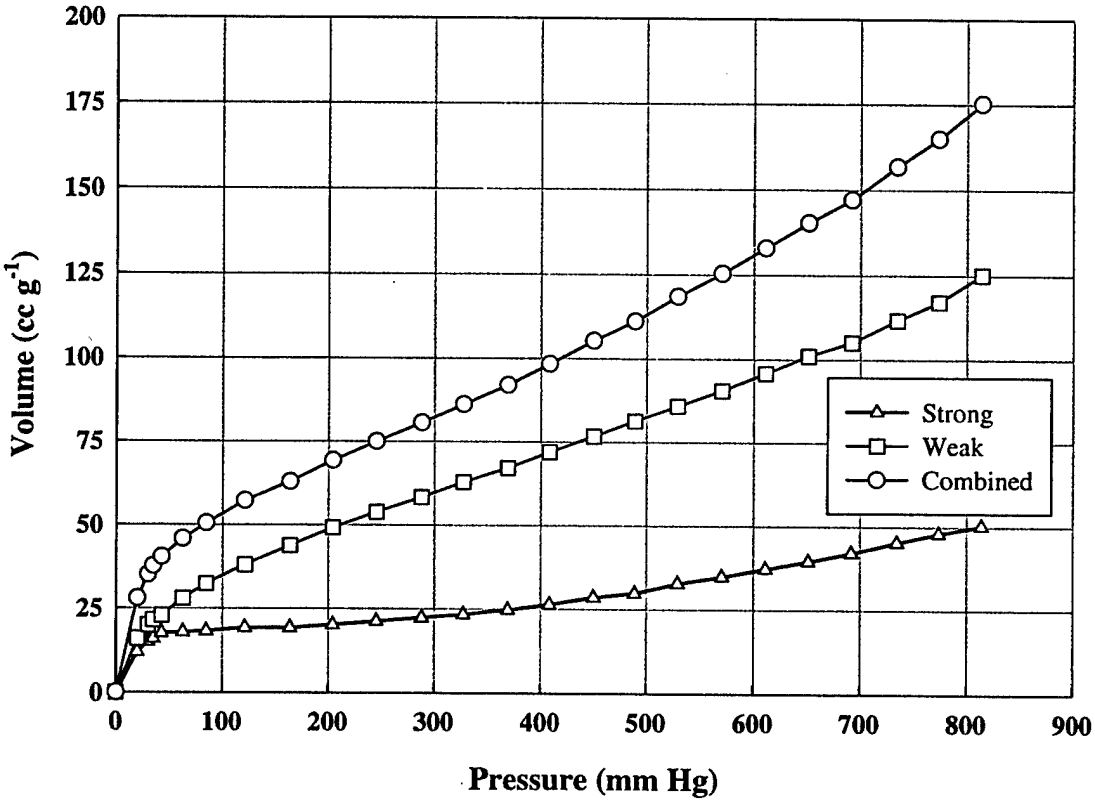

Figure 42. Ammonia adsorption isotherm at 25°C on activated carbon.

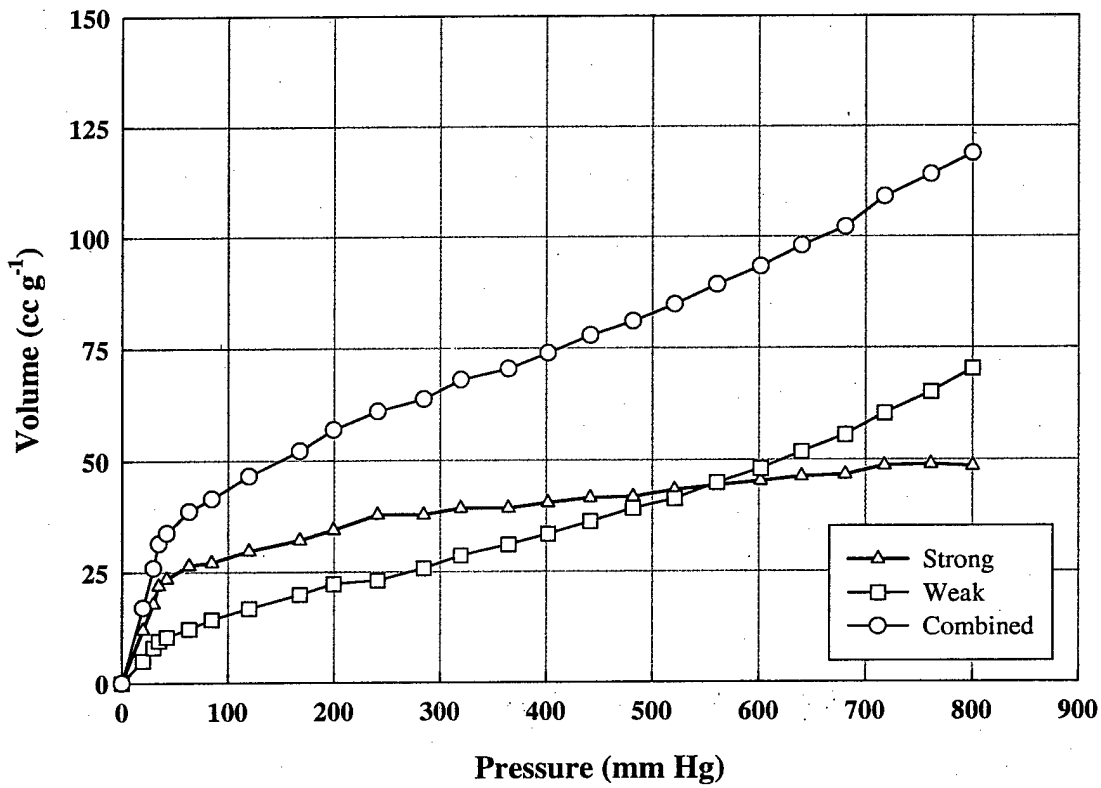

Figure 43. Ammonia adsorption isotherm at 100°C on activated carbon.

D. Ammonia Storage

The fabricated aluminum ammonia storage canister was filled with 130 g of anhydrous ammonia. This mass of ammonia occupied approximately one-half the canister volume on a liquid basis. The canister was simply stored in a fume hood for a period of 17 days upon which it was bubbled through water and subsequently neutralized with sulfuric acid. The canister was then successfully hydrostatically pressure tested to 150 psig. Based on these simple qualitative results, it appears that the aluminum canister sufficed in containing ammonia. Therefore, future work pertaining to the storage of ammonia with aluminum vessels thus seems useful and could very well be promising.

Lastly, the issue of an ammonia storage vessel rupturing is important with respect to safety. Based on adsorption data already presented one could conceivably use a substantial amount of adsorbent to enclose the vessel. Of course this would add substantial weight to the vessel (approximately 9 grams of adsorbent for every gram of ammonia). Another alternative would be to build the canister more robust to prevent a catastrophic rupture. However, this would also add weight. Guidelines will have to be developed in the future to provide insight into the trade-offs between added weight in the form of adsorbent, added weight in the form of thicker canister materials, and the acceptable risk taken by the user of a given ammonia storage vessel.

V. CONCLUSIONS

Overall, the research conducted under this contract was extremely useful in that it allowed for the integration of autothermal ammonia decomposition chemistry into an experimental ammonia-based power system. Aside from the opportunity to verify prior work in autothermally generating hydrogen from ammonia, insight was gained into the challenges of scaling down a reaction system as to reduce its size and weight. In the end, however, definite strides have been attained in developing a small-scale ammonia-based power system. As is usually the case, additional work remains to be done in order to increase the efficiency and reduce the size of the overall system. For example, operation of the reaction system could only be done at ammonia:oxygen ratios of four or less; operating at higher ammonia:oxygen ratios allows less hydrogen to be incorporated into water thus improving the energy-density of the overall system. However, as the ammonia:oxygen ratio is increased less heat is liberated to drive the endothermic decomposition of ammonia. Thus, additional thermal integration of the system is necessary to maximize the energy-density of the system.

Insight has also been gained in the area of storing anhydrous ammonia and its safe use. Anhydrous ammonia can be adequately stored in aluminum canisters. Also, adsorption data indicates that zeolites can be used to sequester residual ammonia leaving the hydrogen-generating catalytic reactor. These adsorbents can also be useful in protecting the vessels anhydrous ammonia is stored.

VI. REFERENCES

1. Vancini, C.A., *Synthesis of Ammonia*. London: Macmillan Press, 1971.
2. Haber, van Oordt, *Z. Anorg. Chem.*, **43,** 111 (1904).
3. Nernst, Jost, Jellinek, *Z. Elektrochem.*, **13,** 521 (1907).
4. Benton, A.F., *Ind. Eng. Chem.*, **19,** 494 (1927).
5. Frankenburger, W., *Z. Elektrochem.*, **39,** 276 (1933).
6. Egawa, C., Nishida, T., Naito, S., Tamaru, K., *J. Chem. Soc., Faraday Trans.*, **80,** 1595 (1984).
7. Loffler, D.G., Schmidt, L.D., *Journal of Catalysis*, **41,** 440 (1976).
8. McGill, W.J., Sebba, F., *Journal of Catalysis*, **2,** 104 (1963).
9. Boffito, C. US Patent 5 976 723, 1999.
10. Love, K.S., Emmett, P.H., *J. Am. Chem.*, **63,** 3297 (1941).
11. Berger, C., *Handbook of Fuel Cell Technology*, New Jersey: Prentice-Hall, Inc., 1968.
12. Appleby, A.J., *Journal of Power Sources*, **53,** 187 (1995).
13. Huff, M., Torniainen, P.M., Schmidt, L.D., *Catalysis Today*, **21**(1), 113 (1994).
14. Flytzani-Stephanopoulos, M., Schmidt, L.D., Caretta, R., *Journal of Catalysis*, **64,** 346 (1980).
15. Pignet, T., Schmidt, L.D., *Chem. Eng. Sci.*, **29,** 1123 (1974).
16. Pignet, T., Schmidt, L.D., *Journal of Catalysis*, **40,** 212 (1975).